بسم الله الرحمن الرحيم

Sudan University of Science and Technology

Faculty of Engineering

Aeronautical Engineering Department

Design Optimization and Analysis for A Vertical Flight Technique (Aerodynamic Analysis)

—Thesis Submitted in Partial Fulfillment of the Requirements for the Degree of Bachelor of Science. (BSc Honor)

By:

Marwa Abbas Abdel Hamid Ali

Supervised By:

Dr. Tariq Mohammed Osman

Co-Supervisor:

Abdel Aziz Abdel Majid Suliman

October,2016

الآية

بسم الله لرحمن الرحيم

(يَا مَعْشَرَ الْجِنِّ وَالْإِنسِ إِنِ اسْتَطَعْتُمْ أَن تَنفُذُوا مِنْ أَقْطَارِ السَّمَاوَاتِ وَالْأَرْضِ فَانفُذُوا ۚ لَا تَنفُذُونَ إِلَّا بِسُلْطَانٍ)

سورة الرحمن الآية (33)

Abstract

This report is about designing new parts that enable the fighters to perform the vertical flight maneuver depending on the fixed wing lift, with minimum fuel consumption and suitable layout for super maneuverability aircrafts (applied at sukhoi-35).

In order to perform this maneuver with minimum fuel consumption and keep suitable layout we had conceptually designed new parts (sliding parts) that kept inside the wing structure and then extent along the semi span, the sliding parts work as storage for the fans. The fans are small diameter fans distributed equally along the semi span stored inside the sliding parts, it's function is to accelerate the flow over the wing thus increasing the wing lift.

All mathematical models of sukoi-35 had been built using calculation and Microsoft office excel 2016, starting with aerodynamic model using thin airfoil theory and aerodynamics all aerodynamic parameters had been calculated, stability model had been estimated and also the structural model. Conceptual design of the sliding parts and fans had been done starting with sizing satisfying the requirements, and both of them had been drown using CATIA v5, then they had been incorporated into the original CAD model of sukhoi-35. Finally, computational aerodynamic analysis had been done using CFD (fluent), and all results had been discussed.

التجريد

هذا البحث يتحدث عن تصميم اجزاء جديدة تمكن الطائرات الحربية من اداء مناورة الطيران العمودي بالاعتماد على الرفع الناتج من الجناح الثابت بأقل تكلفة وقود ممكنه وبالتصميم المناسب للطائرات فائقة المناورة (طبقت على سوخوي-35).

لكي تؤدى هذه المناوره باقل تكلفة للوقود وبالمحافظة على التصميم الخارجي للطائرات الحربيه، قمنا بتصميم اجزاء جديدة تصميما خياليا(اجزاء منزلقة) محفوظة داخل هيكل الجناح وتمتد على مدى طول الجناح، الاجزاء المنزلقة تعمل كمخزن للمراوح. المراوح هي مراوح صغيرة القطر موزعة بإنتظام على مدى طول الجناح مخزنة داخل الاجزاء المنزلقة، وظيفتها تسريع سريان الهواء فوق الجناح وبالتالي زيادة رفع الجناح.

كل النماذج الرياضية للطائرة سوخوي-35 قد تم حسابها باستخدام الحساب او باستخدام برنامج ميكروسوفت اوفيس ايكسيل (2016) ، تم البدء بنموذج الديناميكا الهوائية بإستخدام نظرية مقطع الجناح الرفيع والديناميكا الهوائية وتم حساب كل العوامل الديناميكه الهوائيه ، تم حساب نموذج الاستقرارية ونموذج هيكل الطائرة. تم تصميم الاجزاء المنزلقة والمراوح تخيليا ابتداءا من القياس ومطابقة متطلبات التصميم، بعد ذلك تم رسم كلا من الاجزاء المنزلقة والمراوح في كاتيا 5، بعد ذلك تم دمجهم مع المجسم ثلاثي الابعاد للطاترة سوخوي-35 .اخيرا، تم تحليل الجناح لحساب الديناميكا الهوائية باستخدام ديناميكا الموائع التحسيبية (فلونت) وتمت مناقشة النتائج الناتجة.

Acknowledgement

Thanks first and last to Allah...

I present most of thanks and gratitude to my supervisor Dr. Tariq Abo Rass who helped me in this project...

Also to my teacher Raheeg Wahbi ...

To my teachers in aeronautical engineering department ...

To Mohammed Altegani ...

To my colleges ...

Researcher ...

Dedication

To the virtuous lady … my mother … who teach me to love science and work … god bless you.

To my family …. who care and support.

To my friends … who stand by me, support me and helped a lot in this project…

To Ahmed Albukhary may his soul rest in peace …

I dedicate this work to all of you…

Researcher …

Contents

List of figures

List of tables

List of abbreviations

$\alpha_{L=0}$	Angle of attack at zero lift line.
c	Chord.
a	Lift curve slop.
$\Lambda_{c/2}$	Sweep angle at mid chord.
a_o	Lift curve slop at zero angle of attack.
AR	Aspect ratio.
e	Oswald efficiency factor.
λ	Taper ratio.
C_t	Tip chord.
C_r	Root chord.
e_0	Span efficiency factor.
δ	the induced drag factor.
$\Lambda_{L.E.}$	Leading edge sweep.
$\bar{x}_{ac}$	Location of the aerodynamic center.
$Cm, c/4$	Moment coefficient around the quarter chord.
Λ_{ac}	Sweep angle at the aerodynamic center.
$C_{m,ac}$	Moment coefficient around the aerodynamic center.
M_{ac}	Moment around the aerodynamic center.
$\bar{C}$	Mean aerodynamic chord.
S	Wing area.
ρ	Free stream density.
V	Free stream velocity.
C_D	Drag coefficient.
$C_{D,0}$	Parasite drag coefficient.
$C_{D,i}$	Induced drag coefficient.
$C_{D,w}$	Wave drag coefficient.
C_L	Lift coefficient.
$\Delta C_{D,0}$	The increment in parasite drag coefficient.

$C_{m_{\alpha,wb}}$	Wing –body pitching moment coefficient.
$\bar{x}_{cg,wb}$	Location of the center of gravity of wing –body.
$\bar{x}_{ac_{wb}}$	Location of the aerodynamic center of the wing –body.
$C_{L_{\alpha WB}}$	Lift curve slope of the combined wing body.
K_N	Ratio of nose lift.
$K_{W(B)}$	Ratio wing lift in presence of the body.
$K_{B(W)}$	Ratio wing lift in presence of the body to wing-alone lift.
$C_{L,\alpha e}$	Lift curve slope of exposed wing.
S_{exp}	Exposed wing area.
M	Mach number.
$C_{L_{\alpha,N}}$	lift curve slope for isolated nose.
$b_{f,max.}$	The local width/diameter.
$S_{B,max.}$	Maximum cross sectional area of the body.
b	Wing span.
l_f	Fuselage Length.
C_{re}	Exposed root chord.
l_N	The distance from the LE of fuselage to the LE exposed wing root chord.
η_t	Dynamic pressure ratio.
V_t	Tail volume ratio.
k_A	Wing aspect ratio.
k_λ	Wing taper ratio.
l_h	Distance measured parallel to the wing root chord.
h_H	Height of horizontal tail mac above or below the plane of the wing root chord.
k_H	Horizontal tail location factor.
q	Dynamic pressure.
V_h	volume ratio.
a_t	Tail lift curve slope.

$C_{m_{\alpha,t}}$	Tail pitching moment coefficient.
$M_{CG.propeller}$	Pitching moment around C.G of the propeller.
T_P	Thrust of propeller.
h_p	Normal distance between C.G of propeller and C.G of aircraft.
$C_{m_{CG.R}}$	pitch moment coefficient around the C.G of the rotor.
$C_{m_{\alpha.R}}$	Rotor pitching moment coefficient.
$M_{CG.R}$	pitch moment around the C.G of the rotor.
l_p	Distance between C.G of propeller and C.G of aircraft.
N_P	Number of propellers.
α_p	Angle of attack of propeller.
S_P	Propeller area.
a_{sp}	Sliding part lift curve slope.
$\bar{x}_{cg}$	Location of the center of gravity of the sliding part.
$\bar{x}_{ac_{sp}}$	Location of the aerodynamic center of the sliding part.
$C_{m_{\alpha,sp}}$	Sliding part pitching moment coefficient.
q_s	Shear flow distribution.
q_b	Shear flow distribution at open section.
$q_{s,o}$	Shear flow distribution at origin.
β_r	Boom area.

Chapter one

Introduction

Chapter one: Introduction

1.1 Introduction

There is many maneuver allow the aircraft to translate from an altitude to another by regular climb or by vertical takeoff. Vertical takeoff can be achieved using rotating wing as in helicopter, or fixed wing as in thrust vectoring and ducted fan, or semi fixed (fixed/rotating) wing such the technologies used by NASA (Dos Samara, retracting wing and Trifecta). The climb can be performed at any altitude even reach the absolute ceiling, while the vertical takeoff techniques are performed from the ground into specific altitude. In this project we will bay attention for the vertical takeoff performed by fixed wing and semi fixed wing. [1][2][3][7]

For fixed wings there is two main paths for vertical takeoff, upward normal to the wing and parallel to the wing. The first one is uncommon in spite of that this maneuver done successfully at certain conditions and certain techniques such as jet jump and fan in duct. The jet jump is thrust vectoring technique to rise the aircraft up from the ground at zero x velocity, it depends on engine thrust and some large fans it is uneconomical and has heavier frames. Fan in duct depend on large fan locate in the wing and it used in horizontal flight path because it based in slip stream effect, this technology is unsuitable for fighter's layout in spite of that it is economical. [2][3]

But in this project we focus on the vertical takeoff in NASA techniques which has independent vertical flight system (which work with motors) than the propulsive system (which work with fuel) except in Trifecta concept where the front propeller is both part of the vertical flight and propulsive system. The increasing of the vertical force mainly depends on the DC motors rpm. But the three layouts are not suitable for fighter's layout and requirements. [1][6][7]

This project is a combination between climb which happen at any altitude even reach the limit ceiling and vertical takeoff normal to the fixed wings to produce a technique very similar in conditions to semi fixed NASA technologies but more suitable for fighter layout. We will make the aircraft (sukhoi-35) capable to perform the vertical flight maneuver

normal to the wing depending on the lift produced by the wing and at any altitude even reach the limit ceilings. [2][5][6].

1.2 Aim and Objectives

Aim: To be sure that the aircraft will perform the vertical flight maneuver with high efficiency, performance and with minimum response time.

Objectives:

1. Estimation of the wing mathematical models.
2. Conceptual design and drawing of the new parts (SP, fan) and incorporate it into the SU-35 CAD model.
3. Computational aerodynamic analysis of the new wing combination.

1.3 Problem Statement

Vertical takeoff maneuver is uncommon because of the high energy needed to perform it with jet jump besides the high fuel consumption (engine produces maximum thrust), additional heavy means added to suck air with large masses, and the large fans used as in fan in duct technique which incorporated into the wings is not suitable for super maneuverability fighter's layout.

To reduce the fuel consumption and the time of clime needed by the aircraft to translate through relatively short height and to keep suitable layout for fighters we will make a conceptual design of parts that make the A/C capable to perform the vertical fight maneuver normal to the wing depending on the lift produced by the fixed wing from steady level flight at a wide range of altitudes depending on the concept of slip stream. And incorporate them into the aircraft. And study the effect of the incorporation analytically and computationally.

Also, we will study the effect of this incorporation on the aircraft performance to know the benefits and penalties, also we will study this effect on the aircraft structure, modify the weak parts of the structure as possible and refer to the weak parts.

1.4 Proposed Solution

We will conceptually design a new part (sliding part) for the original wing and incorporate a series of special small diameters NASA fans to accelerate the flow over the

wing to higher Mach number (about 0.4 Mach) in order to decrease the pressure on the upper surface to increase the lift. And make a suitable structural incorporation consider the effect on the performance and the structure and the stability. To make the analytical analysis we will use theoretical equations and to make the computational aerodynamic analysis we will use CFD (fluent) and drawing programs.

1.5 Methodology and Methods

Firstly, data were collected, then the wing combination models were estimated in form of equations analytically starting with aerodynamic model using aerodynamics and thin airfoil theory the aero dynamic model had been built, then structural model was estimated depending on the aerodynamic model force distribution, then a simple stability model had been built to ensure longitudinal stability during maneuver. A conceptual design of the sliding part and fans had been done starting with sizing and satisfying the requirements and then the sliding parts and fan had been drawn in CATIA v5, then both of them had been incorporated with the 3D CAD model of su-35. Then the CATIA new model had been imported into the CFD (fluent) and aerodynamic analysis had been done computationally. The all the results were discussed and compared with the results before the wing modifications.

1.6 Thesis Outline

This thesis contains five chapters, chapter one includes introduction, problem statement, proposed solution, objectives and methodology. Chapter two includes background about similar techniques at different conditions, NASA supersonic through flow fan, slip stream effect and optimization. Chapter three includes su-35 mathematical models (aerodynamic, stability and structural model), sliding part conceptual design, fan conceptual design, and drawing of sliding parts and fans in CATIA v5. Chapter four include the analytical and computational results and discussion. Chapter five includes conclusion, recommendation and future work.

Chapter two

Literature Review

Chapter two: Literature Review

2.1 History and Background About Fixed Wing Vertical Takeoff

2.1.1 Thrust Vectoring

Also thrust vector control or TVC, is the ability of an aircraft, rocket, or other vehicle to manipulate the direction of the thrust from its engine(s) or motor(s) in order to control the attitude or angular velocity of the vehicle. [26]

In rocketry and ballistic missiles that fly outside the atmosphere, aerodynamic control surfaces are ineffective, so thrust vectoring is the primary means of attitude control.

For aircraft, the method was originally envisaged to provide upward vertical thrust as a means to give aircraft vertical (VTOL) or short (STOL) takeoff and landing ability. Subsequently, it was realized that using vectored thrust in combat situations enabled aircraft to perform various maneuvers not available to conventional-engined planes. To perform turns, aircraft that use no thrust vectoring must rely on aerodynamic control surfaces only, such as ailerons or elevator; craft with vectoring must still use control surfaces, but to a lesser extent. [26]

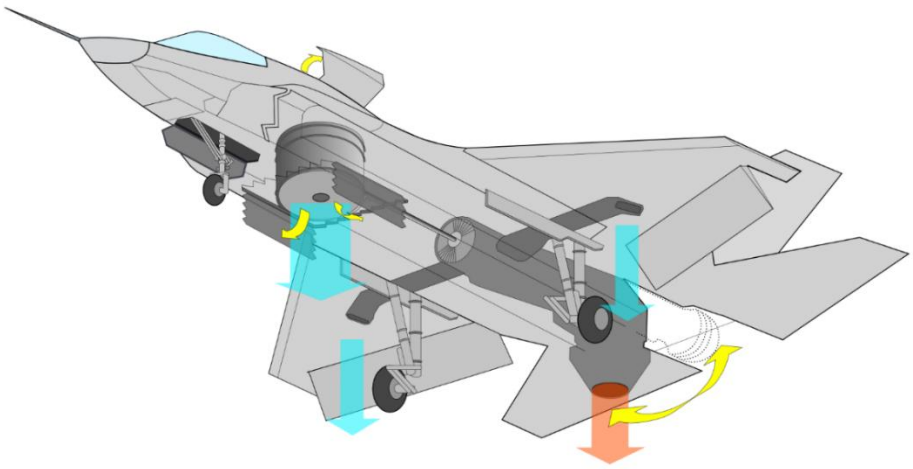

Figure 1: thrust vectoring technique.

2.1.2 Ducted Fan Aircraft

Another idea shine during 1950s/1960s in USA, is the Fan-in-wing. The vertical takeoff and landing achieved through a large fans lies in large holes in the fixed wing. In the forward flight, the fans rotate by 90 degrees in a position seem likes conventional turboprop. [19]

The first representation of the fan-in- wing was coupled with the flying saucer (circular flying wing). The first project was Avro Canada Avrocar which established by USA in 1950. [19] [20]

A ducted fan is a propulsion arrangement whereby a mechanical fan, which is a type of propeller, is mounted within a cylindrical shroud or duct. The duct reduces losses in thrust from the tips of the props, and varying the cross-section of the duct allows the designer to advantageously affect the velocity and pressure of the airflow according to Bernoulli's Principle. Ducted fan propulsion is used in aircraft, airships, airboats, hovercraft and fan packs.

Ducted fans normally have more and shorter blades than propellers and thus can operate at higher rotational speeds. [3]

Figure 2: ducted fan aircraft.

Advantages:

- By reducing propeller blade tip losses, the ducted fan is more efficient in producing thrust than a conventional propeller of similar diameter, especially at low speed and high static thrust level (airships, hovercraft).
- By sizing the ductwork appropriately, the designer can adjust the air velocity through the fan to allow it to operate more efficiently at higher air speeds than a propeller would.
- For the same static thrust, a ducted fan has a smaller diameter than a free propeller, allowing smaller gear.
- Ducted fans are quieter than propellers: they shield the blade noise, and reduce the tip speed and intensity of the tip vortices both of which contribute to noise production.
- Ducted fans can allow for a limited amount of thrust vectoring, something normal propellers are not well suited for. This allows them to be used instead of tiltrotors in some applications.
- Ducted fans offer enhanced safety on the ground. [3]

Disadvantages:

- Less efficient than a propeller at cruise (at lower thrust level).
- Good efficiency requires very small clearances between the blade tips and the duct.
- Requires high RPM and minimal vibration.
- Complex duct design, and weight increase even if constructed from advanced composites.
- At high angle of attack, parts of the duct will stall and produce aerodynamic drag.[3]

2.1.3 Focke-Achgelis Fa 269

Conceived as a single-seat fighter, the Fa 269 project resulted from a design study order issued by the Reich Air Ministry to Focke-Achgelis in 1941. The order called for a local defense fighter which would combine the VTOL capabilities of a helicopter with the speed and economy of a conventional fixed-wing aircraft. A large amount of wind tunnel testing was undertaken, along with work on gearboxes, drives and power-pivoting

mechanisms, and a full-scale mock-up of the aircraft was built to demonstrate the VTOL concept, but much of this was destroyed by Allied bombing raids and all work was shelved in 1944 when Focke-Achgelis estimated that there was little likelihood of a practical prototype being available before 1947.

A mid-wing monoplane, the Fa 269 was to have been powered by a single BMW 801 air-cooled radial engine buried in the fuselage behind the cockpit, which was to have driven transverse drive shafts in the leading edges of the fixed wing, the shafts turning three-bladed rotors via synchronized gearboxes. The plane of rotation of the rotors would have been capable of being swiveled through 80° using angled extension shafts.

It was proposed that the Fa 269 would adopt a high angle of attack when at rest using extremely long undercarriage units. For vertical take-off, the rotors would be lowered till their plane of rotation was parallel with the ground. For translation to conventional flight following take-off, the extension shafts were to pivot to the rear, the rotors then behaving as pusher propellers. [23]

Figure 3: Focke-Achgelis Fa 269

2.2 History and Background About Fixed/Rotating Wing Vertical Takeoff

For semi fixed wings NASA develop three prototypes based on three similar concepts: Dos Samara, retracting wing and Trifecta technologies. All the three concepts are established in a program to develop a long endurance vertical takeoff vehicle can takeoff

of until 18000 meter so they try to decrease the fuel consumptions through weight decreasing. [6]

2.2.1 Dos Samara

Dos Samara has "outboard wing panels, which spin to generate thrust to lift the vehicle in vertical flight. In horizontal flight, the outboard wing panels lock. A pusher propeller is located on the tail to provide forward thrust in horizontal flight" fig (4). [6]

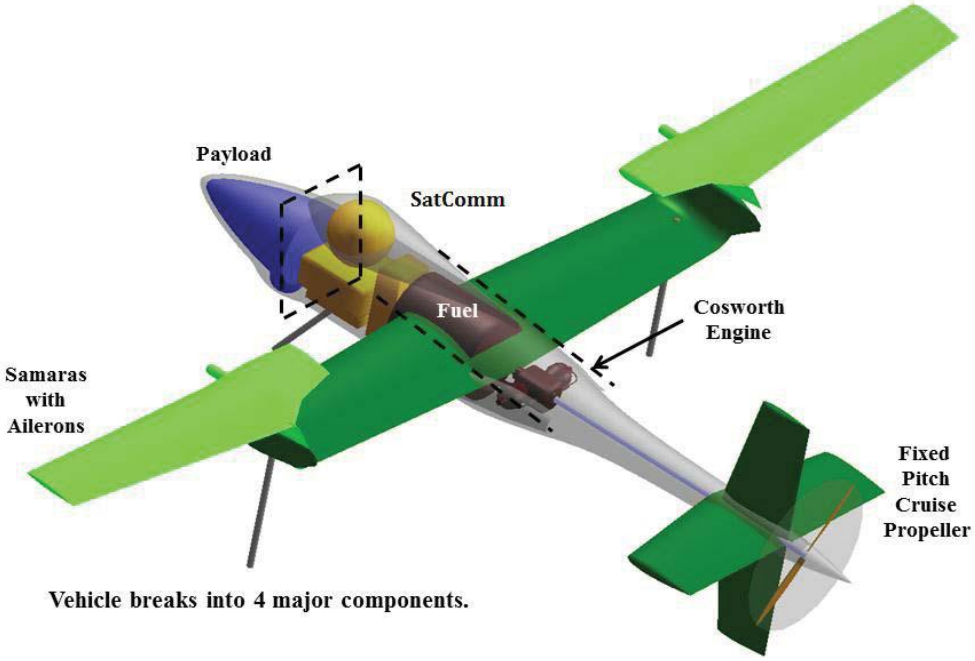

Figure 4: dos samara.

2.2.2 Retracting Rotor

Retracting rotor has a rotor completely retracted to the fuselage at horizontal flight while extended out in vertical flight. A pusher propeller also used to produce thrust in horizontal flight fig (5). [6]

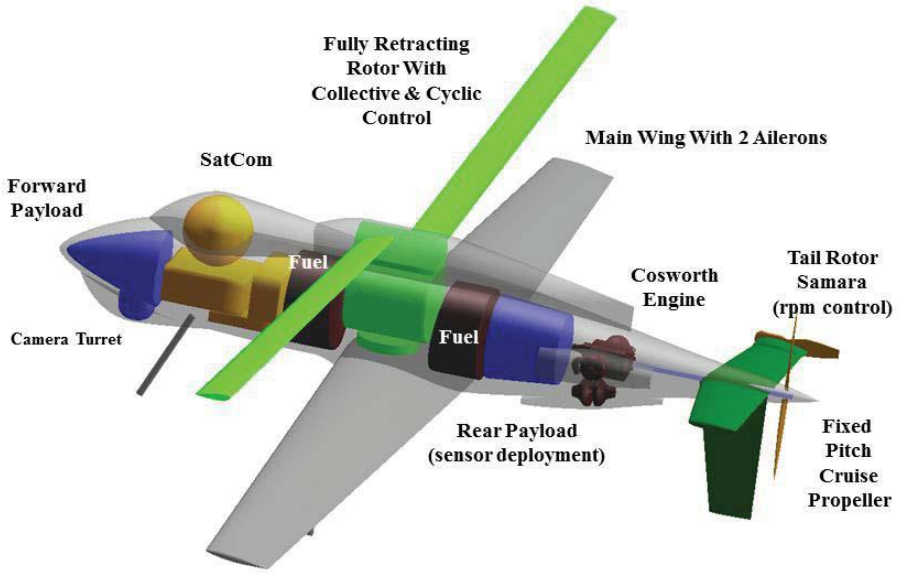

Figure 5: retracting rotor.

2.2.3 Trifecta

The Trifecta is a tri-copter vehicle which has a front propeller connected to a diesel engine which rotate 90 degrees to produce the lift at the nose in the vertical flight. Also two mono blade lift propellers are adding at the tip of the horizontal tail to produce the lift in the vertical flight at the rear, this blades rotating with direct electrical motors, fig (6). "The elevators deflect 90 degrees trailing edge down in hovering in order to reduce the download on the horizontal tail". [6]

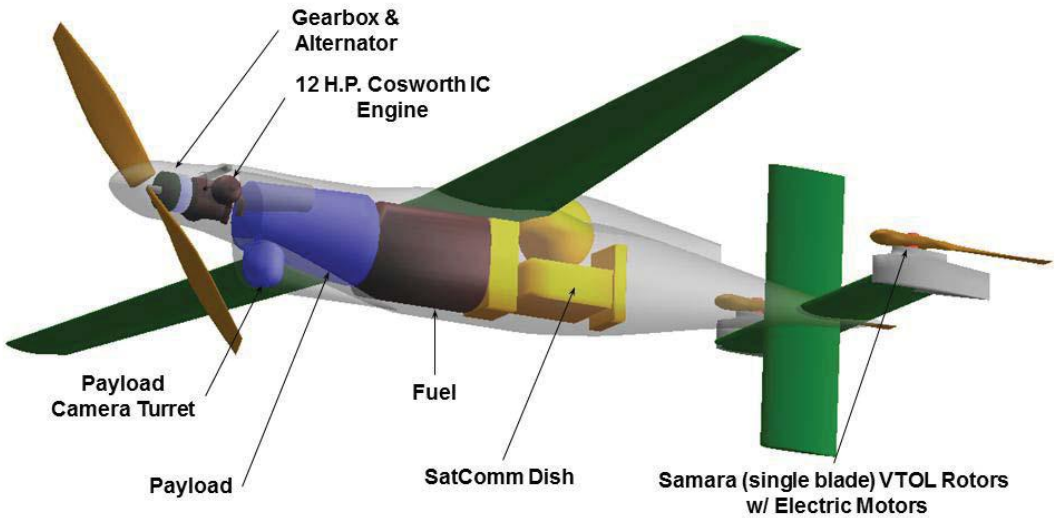

Figure 6: trifecta.

2.3 Background on the techniques that increase the fixed wing lift at low aircraft speed

2.3.1 Morphing wing

The morphing wing are the wings that can change their shapes under the command of control. They have been used to satisfy certain purposes such as increasing the wing lift through changing the wing geometrical parameters (wing area planform, the wing aspect ratio, the leading edge radius …etc.). [15] [25]

A way using the morphing wing was used to improve the airfoil low speed performance (stall limit) is by increase the leading edge radius and the thickness chord ratio. The problem with this is the worse airfoil performance at the high speeds. [25]

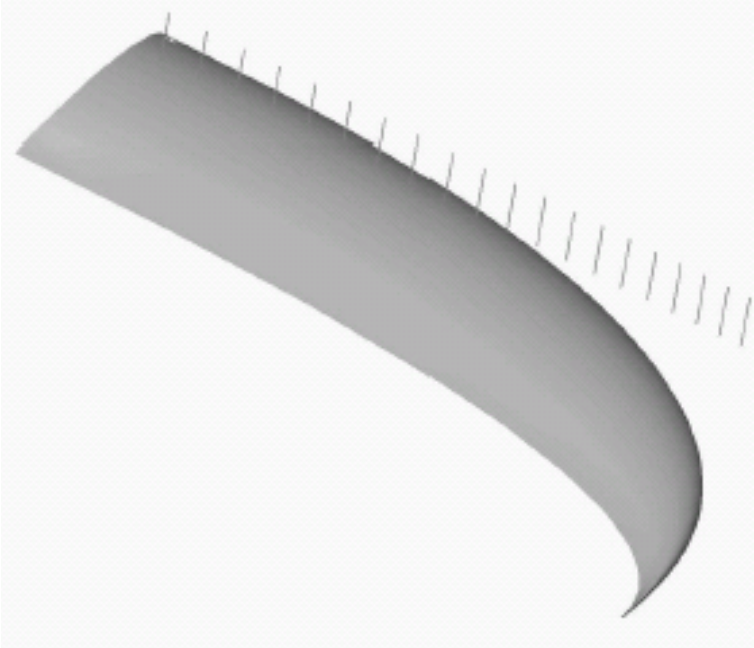

Figure 7: application to hyper-elliptical cambered span.

Many complex morphing shapes can be achieved using advanced morphing mechanism such as the complex shape: hyper-elliptical cambered span, see figure (7). A complex sliding rib structure has been developed by Cornerstone Research Group, Inc. to "vary the planform area and aspect ratio of a wing. The structure consists of sliding wing boxes that can move forward, backwards and outwards in the wing thus increasing the net

planform for the wing. The choice of for the structure is not clear but inchworm motors and piezoelectric actuators are considered as preferred choices. However, these actuators will need to be coupled to other mechanisms to increase their overall strain to achieve significant aerodynamic benefits of wing morphing" see the figures (7) (8). [25]

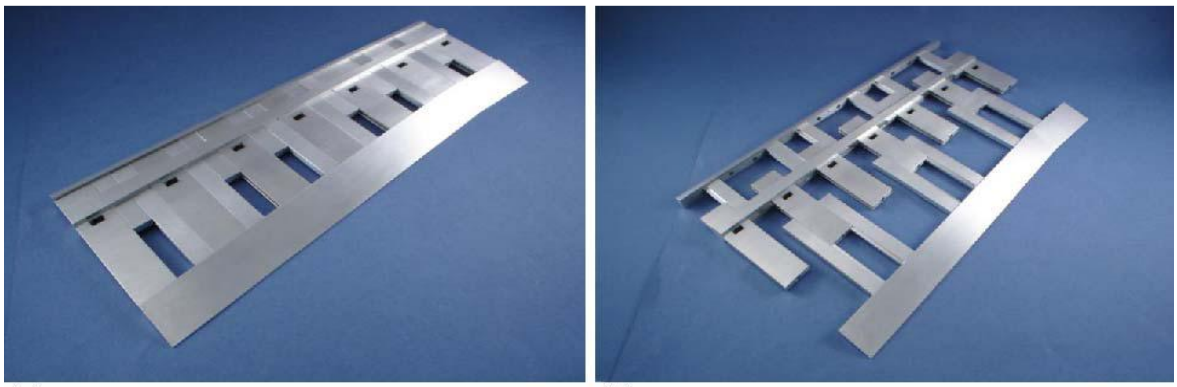

Figure 8:(a) Closed Configuration of Corner Stone Wing. (b) Open Configuration

.

2.4 History and Background About Supersonic Through Flow Fan (STF Fan)

To prove the concept, the STF fan experimentally (maintain a supersonic flow through compression system with only weak shock waves flow losses) NASA Lewis research center embarked a program contain the design of STF fan using four advanced computational codes due to the lack in the experimental data base to depend on it in the design. The other part of the program is the test of fan using a modified multi-stage compressor facility to be suitable for the new fan design. [7]

Table 1:NASA supersonic(design conditions).

Pressure ratio	2.45
Weight flow, lb/sec	31 .5
Inlet axial Mach number	2.0
Tip speed, ft/sec	1 500
rotation speed, rpm	17 189
Diameter, in.	20
Hub-tip ratio	0.7

As any traditional fan, STF fan stage consist of rotor and stator. The stator is designed to eliminate the swirl of the rotor.

Table 2: rotor and stator design parameters.

	Rotor	Stator
Rotation speed	17 188.7 rpm	-
Total pressure ratio	2.1	-
Tip radius, constant. in .	10	10
Hub radius, constant, in .	7	7
Blade number	44	52
Aero-chord, in .	4.45 (tip) to 3.56 (hub)	3.65 (tip) to 3.28 (hub)
Aspect ratio , span to mean chord ratio	0.97	0.86
Solidity , blade chord to spacing ratio	3.11 (tip) to 3.56 (hub)	3.02 (tip) to 3.88 (hub)
Maximum thickness/chord, percent	4 to 7	5
Leading edge thickness/chord. percent	0.15 to 0.19	0.14 to 0.15
trailing edge thickness/chord, percent	0.27 to 0.037	0.27
Leading edge radius, in	0.005	

Rotor design

The establishing of the rotor velocity diageram was the step that follow the specifiction setting; because it "specify the mass f low and energy addition given the wheel speed and f low path geometry" table (3), figure (9). [7]

Table 3: hub and tip description.

	Tip	Hub
Relative tip Mach number	2.7	2.36
Flow turning by	32 deg.	22.6 deg.

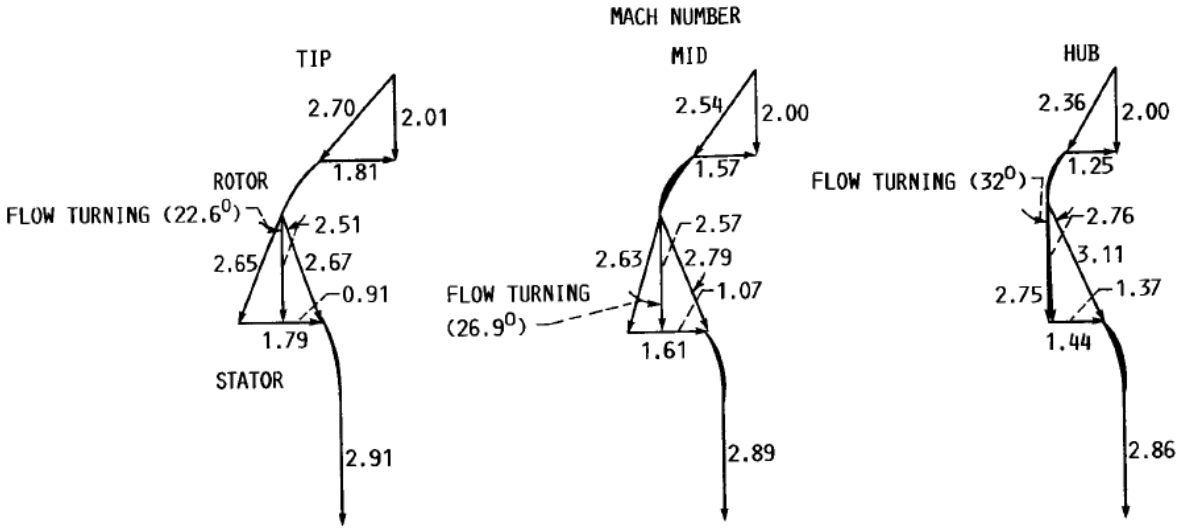

Figure 9: NASA STF fan vector diagram.

The solidity, the chord and the thickness ratio of the tip and the hub was chosen in a compromising way to be sure the upper and the lower surface static pressure at the trailing edge was matched (equally) "then the f low can leave the blade almost tangent to the blade angle and no large e adjustments (such as shock waves) to the flow are necessary at the trailing edge or downstream of the blade row." also to be sure a good blade performance and mechanical stresses within the acceptable limit at the hub also to be sure the relatively thick hub didn't cause any strong shock waves at the leading edge which result in a poor aerodynamic performance. [7] Table (4) describe the tip and the hub.

Table 4: hub and tip description.

	Blade solidity	Max. Thick. Chord	Blade chord (in)
Hub	3.56	0.07	3.56
Tip	3.11	0.04	4.45

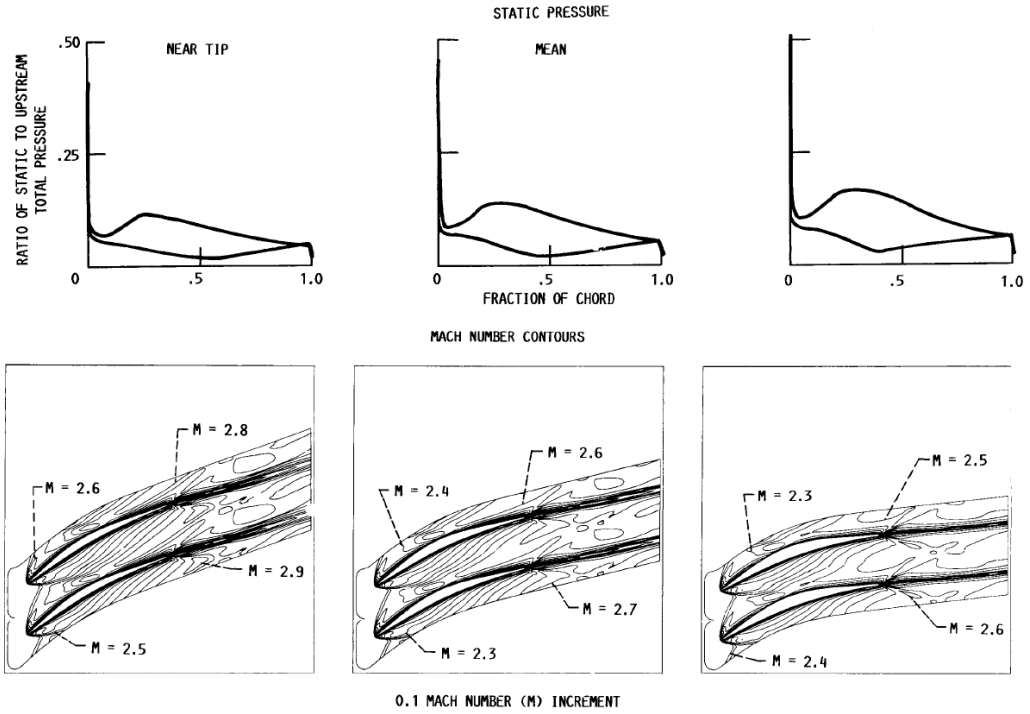

Figure 10:Mach number increment at tip, mid and hub section.

"The blade angle distribution was varied to fine tune the flow distribution over the blade"." a fairly sudden rise in blade angle near the leading edge which was used to decrease the leading edge wedge angle in order to reduce the strength of the leading edge shock wave. This rise was followed by a rapidly decreasing blade angle until mid-chord. The rear half of the blade had a linear blade angle distribution which produced a large static pressure gradient on the suction surface and practically no loading over the last 25 percent of the blade. The effect of the static pressure gradient on the suction surface is evident on the contour plot of Mach number by a significant increase in the viscous dominated region downstream of the location where a weak shock impacts the surface at about 50 percent of the chord". [7]

"Ferri was the first one to indicate the potential advantages of high fan pressure ratio (in single stage) and elimination of the subsonic portion of the supersonic inlet with the use of an STF fan. Franciscus showed that the STF fan equipped engine would significantly reduce specific fuel consumption compared with a conventional turbofan engine for a supersonic cruise mission. For a supersonic transport operating at Mach number of 2.7, Tavares suggests that an STF fan efficiency of only 68 percentages is

necessary to have performance advantage over a turbojet engine. These estimates of performance improvement from the cycle studies were based on assumed characteristics of the STF fan obtained from transonic fan data" [7].

"All these cycle studies have an inherent uncertainty because of the lack of experimental data for the STF fan. A prototype STF fan rotor was designed, built, and tested by Breuge lmans. However, before the design speed could be attained a blade failure was encountered and the limited data obtained was insufficient to determine if supersonic through-flow was achieved" [7].

"Considering the large potential advantages of using a STF fan in advanced propulsive systems, NASA Lewis has embarked on a program to experimentally prove the concept of an STF fan system" [7].

2.5 Back ground about slip stream effect

A slipstream is a region behind a moving object in which a wake of fluid (typically air or water) is moving at velocities comparable to the moving object, relative to the ambient fluid through which the object is moving.[1] The term slipstream also applies to the similar region adjacent to an object with a fluid moving around it. "Slipstreaming" or "drafting" works because of the relative motion of the fluid in the slipstream.[24]

A slipstream created by turbulent flow has a slightly lower pressure than the ambient fluid around the object. When the flow is laminar, the pressure behind the object is higher than the surrounding fluid.[24]

The shape of an object determines how strong the effect is. In general, the more aerodynamic an object is, the smaller and weaker its slipstream will be. For example, a box-like front (relative to the object's motion) will collide with the medium's particles at a high rate, transferring more momentum from the object to the fluid than a more aerodynamic object. A bullet-like profile will cause less turbulence and create a more laminar flow.[24]

A tapered rear will permit the particles of the medium to rejoin more easily and quickly than a truncated rear. This reduces lower-pressure effect in the slipstream, but also increases skin friction (in engineering designs, these effects must be balanced).[]

The term "slipstreaming" describes an object traveling inside the slipstream of another object (most often objects moving through the air though not necessarily flying). If an object is inside the slipstream behind another object, moving at the same speed, the rear object will require less power to maintain its speed than if it were moving independently. In addition, the leading object will be able to move faster than it could independently, because the rear object reduces the effect of the low-pressure region on the leading object. [24]

2.6 History and background about the optimization

"**Optimization** is an important tool in making decisions and in analyzing physical systems. In mathematical terms, an **optimization problem** is the problem of finding the best solution from among the set of all feasible solutions". [12]

"In spite of these developments, little progress has been made in creating computational tools to aid in the concept finding and early conceptual design phases. A great challenge to engineers carrying out this sensitive activity is not necessarily to conceive a realistic clean sheet airplane design but to convince project management that the best feasible concept complying with market needs is being proposed. Although it is often argued that there exists no substitute for the expert's insight based on former projects, widespread effort is devoted to improving formalized optimization methods. A basic problem is that the choice of a single figure of merit (FOM) defining the design quality is inadequate and even multi-objective optimization is not always the panacea. At the same time, the availability of sophisticated numerical analysis methods and optimization algorithms running on fast and cheap computers is tempting the inexperienced novice to try exercises generating irrelevant or even misleading results. In order to avoid this situation, advanced design managers should have an understanding of modern optimization tools for multidisciplinary tasks. The aim of this chapter is to offer an elementary introduction for non-specialists to approaches that have proven effective in conceptual design" [15].

2.6.1 Classical optimization methods

1. Equational approach

"Equational approaches involve efforts to write meaningful governing equations and solve them mathematically or procedurally. In 1933 Prandtl included wing weight effects in an optimization of span wise lift distribution, yielding a greater loading towards the root than in his own classic elliptical aerodynamic optimization. Göthert in 1939 developed analytical methods to optimize a wing, using span and area as variables. Typical modern analytical optimizations based on derivatives of governing equations can be found in Torenbeek among others". [14]

2. Parametric approach

"In parametric optimization, the selected design parameters such as wing sweep or aspect ratio are varied about the baseline values as seen on the design layout. Estimates are made as to the impact of those variations on the design layout, either by actually having a designer redraw the aircraft for each variation or by applying some selected procedures for automated redesign. These attempt to determine the impacts of parametric design variations without a man-in-the-loop drawing revision. Then, the design is re-analyzed and re-sized, and all performance and cost estimates are recalculated. From this data, an optimum is found using methods ranging from a simple single-variable graph to the sophisticated MDO techniques". [14]

2.6.2 Optimization elements and terminology

1. Objective function

"is a scalar function of the design variables that is to be minimized or maximized during the optimization" [15].

2. Design parameters

The design parameters are the design's variable, unknown and controllable properties and quantities which we want to find their values in a way that maximize or minimize the objective function and vitrify the constrains [10] [13] [15]. The design parameters such as the wing span. It is important to specify how the design

parameters defining the values of the properties and the quantities to categorize them during the computational process [15] as shown below:

- **Pre-assigned parameters:** they are the properties and the quantities which stated by the designer to be constant during the optimization. They derived from such as the design requirement or the previous experience [15].
- **Independent variables are parameters:** they called also selection variables and they are the parameters which ranged between maximum and minimum values [15]. They subdivided into:
    - Integers: known also as discrete, when the selection variables are integers [10] [15] such as the number of ribs.
    - continuous: when the selection variables "can be defined by any real number in a specific interval" such as the wing area [15].
    - Boolean: "such as whether to build a monoplane or a biplane" [10].
- **Dependent variables:** – "also known as behaviour variables – are parameters generated by the design (optimization) process. Forming the outcome of design analysis, their values are controlled by the selection variables. Typical dependent design variables are geometric parameters derived from geometric selection variables, weight and inertia moments of airframe components, aerodynamic parameters such as lift and drag coefficients and stability derivatives, and numbers characterizing the impact on the environment of aircraft operation" [15].

3. Constraints

"Constraints are functions of the design variables representing limitations imposed upon the design" [15]. The constrain "must be satisfied in order for the design to be feasible" [10]. They are divided into:

- **Equality constraint:** where two variables are set to be equality. "Many sizing conditions are translated into equations acting as equality constraints. For example, the condition that in straight and level flight T = D can be interpreted as: 'In a specified flight condition and cruise rating, engines are sized to deliver the thrust required to balance drag.'" [15].
- **Inequality constraint:** is a condition which is almost function in the independent variables to be sure a feasible design is estimated by the optimization process. For

example, “the condition that the wing must have enough volume to contain all the fuel required for a specified long range mission. Depending mainly on wing planform shape and mean thickness ratio, this constraint leads to a lower limit for the wing area” [15].

- **Side constraint:** is to range the selection variables between upper and lower limits [15].

4. **Design space.**

2.6.3 Types of optimization problems

1. **Continuous optimization versus discrete optimization problems**

The continuous optimization is defined as a process where the objective to be optimized is expressed as a function of real variables. while the discrete optimization is encountered with the integer variables [11].

2. **None, single or multi-objectives optimization problems**

The non-objective problem is that, when “the goal is to find values for the variables that satisfy the constraints of a model with no particular objective to optimize” [11]. The single objective problems are encounter with single objective to represent the overall quality of the design [15]. The multi-objectives problems are “when optimal decisions need to be taken in the presence of trade-offs between two or more conflicting objectives. For example, developing a new component might involve minimizing weight while maximizing strength or choosing a portfolio might involve maximizing the expected return while minimizing the risk.” [11].

3. **Unconstrained Optimization versus Constrained Optimization**

“Another important distinction is between problems in which there are no constraints on the variables and problems in which there are constraints on the variables. Unconstrained optimization problems arise directly in many practical applications; they also arise in the reformulation of constrained optimization problems in which the constraints are replaced by a penalty term in the objective function. Constrained optimization problems arise from applications in which there are explicit constraints on the variables. The constraints on the variables

can vary widely from simple bounds to systems of equalities and inequalities that model complex relationships among the variables. Constrained optimization problems can be furthered classified according to the nature of the constraints (e.g., linear, nonlinear, convex) and the smoothness of the functions (e.g., differentiable or non-differentiable)". [11]

4. **Deterministic Optimization versus Stochastic Optimization**

"In deterministic optimization, it is assumed that the data for the given problem are known accurately. However, for many actual problems, the data cannot be known accurately for a variety of reasons. The first reason is due to simple measurement error. The second and more fundamental reason is that some data represent information about the future (e. g., product demand or price for a future time period) and simply cannot be known with certainty. In optimization under uncertainty, or stochastic optimization, the uncertainty is incorporated into the model. Robust optimization techniques can be used when the parameters are known only within certain bounds; the goal is to find a solution that is feasible for all data and optimal in some sense. Stochastic programming models take advantage of the fact that probability distributions governing the data are known or can be estimated; the goal is to find some policy that is feasible for all (or almost all) the possible data instances and optimizes the expected performance of the model".

2.6.4 Optimization process

1. Constructing a Model (problem formulation)

"modeling is the process of identifying and expressing in mathematical terms the objective, the variables, and the constraints of the problem". [13]

"Problem formulation is normally the most difficult part of the process. It is the selection of design variables, constraints, objectives, and models of the disciplines. A further consideration is the strength and breadth of the interdisciplinary coupling in the problem". [10]

"The designer must also choose models to relate the constraints and the objectives to the design variables. These models are dependent on the discipline involved. They may

be empirical models, such as a regression analysis of aircraft prices, theoretical models, such as from computational fluid dynamics, or reduced-order models of either of these. In choosing the models the designer must trade off fidelity with analysis time". [10]

2. Express the problem in the standard form

"Once the design variables, constraints, objectives, and the relationships between them have been chosen, the problem can be expressed in the following form:
find $\mathbf{x}$ that minimizes $J(\mathbf{x})$ subject to $\mathbf{g}(\mathbf{x}) \leq \mathbf{0}$, $\mathbf{h}(\mathbf{x}) = \mathbf{0}$ and $\mathbf{x}_{lb} \leq \mathbf{x} \leq \mathbf{x}_{ub}$ where J is an objective, $\mathbf{x}$ is a vector of design variables, $\mathbf{g}$ is a vector of inequality constraints, $\mathbf{h}$ is a vector of equality constraints, and $\mathbf{x}_{lb}$ and $\mathbf{x}_{ub}$ are vectors of lower and upper bounds on the design variables. Maximization problems can be converted to minimization problems by multiplying the objective by -1. Constraints can be reversed in a similar manner. Equality constraints can be replaced by two inequality constraints".[10]

3. Determining the Problem Type

The third step in the optimization process is "determining in which category of optimization your model belongs" [13]

4. The choice of optimization strategy

5. Selecting Software

The fifth step in the optimization process is "selecting software appropriate for the type of optimization problem that you are solving. Optimization software comes in two related but very different kinds of packages:

5. **Solver software** is concerned with finding a solution to a specific instance of an optimization model. The solver takes an instance of a model as input, applies one or more solution methods, and returns the results.
6. **Modeling software** is designed to help people formulate optimization models and analyze their solutions. A modeling system takes as input a description of an optimization problem in a symbolic form and allows the solution output to be viewed in similar terms; conversion to the forms required by the algorithm(s) is done internally. Modeling systems vary in the extent to which they support importing data, invoking solvers, processing results, and integrating with larger

applications. Modeling systems are typically built around a modeling language for representing the problem in symbolic form. The modeling language may be specific to the system or adapted from an existing programming or scripting language." [13]

"Most modeling systems support a variety of solvers, while the more popular solvers can be used with many different modeling systems. Because packages of the two kinds are often bundled for convenience of marketing or operation, the distinction between them is sometimes obscured, but it is important to keep in mind when attempting to sort through the many alternatives available". [13]

2.6.4.1 How to control the optimization process?

"The number of independent variables reflects the design freedom and is called the dimensionality of the design space, their upper and lower values limit the boundary domain" [15]. Also, it is easier to solve the continuous optimization [10].

"In principle, every combination of selection variables leads to a design analysis resulting in a set of behavior variables which together represent a unique aircraft design. Addition of a new selection variable will increase the design space by one dimension, that is, another set of designs is generated and included in the optimization process" [15]. as a result, the optimization process takes more time and the need of more powerful computers increase. One easier solution to reduce the time and the complexity is by the designer himself by make assumption for some variables values [15].

"An equality constraint may be imposed on a behavior variable such as the design mission range. Such a constraint reduces the number of variables by one and thereby eliminates one dimension from the design space" [15].

"An inequality constraint reduces the size of the design space so that certain combinations of independent variables need not be considered" [15].

"An active constraint is an equality constraint or an exactly satisfied inequality constraint. A feasible design is a vector of values for the selection variables that satisfies all the constraints. The complete collection of feasible points is called the feasible region" [15].

"Continuous optimization problems tend to be easier to solve than discrete optimization problems; the smoothness of the functions means that the objective function and constraint function values at a point [Math Processing Error] can be used to deduce information about points in a neighborhood of [Math Processing Error]. However, improvements in algorithms coupled with advancements in computing technology have dramatically increased the size and complexity of discrete optimization problems that can be solved efficiently. Continuous optimization algorithms are important in discrete optimization because many discrete optimization algorithms generate a sequence of continuous subproblems". [11]

"In practice, problems with multiple objectives often are reformulated as single objective problems by either forming a weighted combination of the different objectives or by replacing some of the objectives by constraints". [11]

2.6.5 Optimization approaches

2.6.5.1 Pareto front

"A further complication is that sometimes a group of such objectives, linked to the same geometry parameters, are in conflict with each other. The solution in such cases is not a single design variable vector that maximizes or minimizes an objective, but rather a hypersurface of designs, which represent equally valid compromises between optimizing the various objectives. These are referred to as Pareto surfaces or Pareto fronts" [16].

"A key limitation of the Pareto approach is the curse of dimensionality in a slightly different guise. When the number of competing objectives exceeds three or four, building the Pareto trade-off surface becomes rather expensive. Moreover, it becomes next to impossible to visualize in an intuitive manner" [16].

"A typical case of the curse of dimensionality precluding Pareto analysis in aircraft design is the treatment of multipoint cases. These commonly appear when multiple flight conditions have to be considered. A classic example is having to optimize cruise and holding/loitering fuel burn simultaneously, each at several points during a mission with different fuel and payload weights, as well as at a range of different density altitudes. The multiplicity of off-design conditions is a particularly pressing concern in the case of high-

speed transports, where sets of design conditions can feature significantly different Mach numbers" [16].

"While the mathematical formalism of the problem is simple – a compound objective function is usually generated as a linear combination of sub-objectives corresponding to the various design points – the solution is not. The difficult part is selecting the appropriate weight for each term of the linear combination. There is no silver bullet solution at present, though there are some promising lines of research (e.g. a method involving weights that adapt to the problem as the optimization progresses, developed by Buckley et al. (2010))" [16].

2.6.6 Optimization methods

1. Surrogate model based methods

"A **surrogate model** is an engineering method used when an outcome of interest cannot be easily directly measured, so a model of the outcome is used instead. Most engineering design problems require experiments and/or simulations to evaluate design objective and constraint functions as function of design variables. For example, in order to find the optimal airfoil shape for an aircraft wing, an engineer simulates the air flow around the wing for different shape variables (length, curvature, material, ...). For many real world problems, however, a single simulation can take many minutes, hours, or even days to complete. As a result, routine tasks such as design optimization, design space exploration, sensitivity analysis and what-if analysis become impossible since they require thousands or even millions of simulation evaluations". [12]

"One way of alleviating this burden is by constructing approximation models, known as surrogate models, response surface models, metamodels or emulators, that mimic the behavior of the simulation model as closely as possible while being computationally cheaper to evaluate. Surrogate models are constructed using a data-driven, bottom-up approach. The exact, inner working of the simulation code is not assumed to be known (or even understood), solely the input-output behavior is important. A model is constructed based on modeling the response of the simulator to a limited number of intelligently chosen data points. This approach is also known as behavioral modeling or black-box modeling,

though the terminology is not always consistent. When only a single design variable is involved, the process is known as curve fitting".[12]

"Though using surrogate models in lieu of experiments and simulations in engineering design is more common, surrogate modelling may be used in many other areas of science where there are expensive experiments and/or function evaluations". [12]

So in other word, "Surrogate modeling is a procedure for reducing computational cost in optimization by representing the high fidelity analysis methods mathematically. The high fidelity methods are sampled across a predetermined set of design variables. The surrogate models utilize the sample data to mathematically represent the design space. Optimization solutions can be rapidly obtained. For these reasons, surrogate models are widely implemented in design optimization [132]. However, surrogate models only approximate the true system equations, and therefore introduce uncertainty". [9]

"The optimum designs obtained using surrogate models may be found to be infeasible when the design is subjected to high fidelity analysis methods. RBDO can be used to manage the uncertainties introduced by surrogate models in order to increase the confidence a designer may place in an optimization solution obtained using surrogate models". [9]

2.6.7 Design optimization

"Design optimization refers to computational methods used to search for designs that are as efficient and effective as possible. The mathematical statement of design optimization problems takes the form of an objective function that calculates a value that represents the critical measure of design performance or merit. The optimum design is the design that is found to have a minimum merit function while satisfying all constraints. Constraints are formulated as statements of equality or inequality that must be satisfied to keep the design feasible. Additionally, search boundaries are usually specified". [10]

2.6.8 Multi-Disciplinary Design Optimization

"MDO can be defined as "a methodology for the design of systems in which strong interaction between disciplines motivates designers to simultaneously manipulate variables in several disciplines [16]." Independent optimizations of individual disciplines

considering local goals does not guarantee an optimum overall design, which requires the consideration of the synergy between each contributing analysis method [16]. Modern engineering optimization has reached a level of complexity that nearly always requires a strategy to handle many coupled disciplines. Inter-disciplinary coupling occurs when the output of one analysis package is required as input for another independent analysis package. This creates a more complex computational problem than single-discipline optimization. Aerospace conceptual design presents a classic example of a coupled system." [10]

Fig (10)" shows the interaction between disciplines for a hypothetical aircraft conceptual design process [41]. System design variables are shared by all disciplines and denoted by Z. Local variables, X, are specific to individual disciplines and Y denotes the information pathway from one discipline to another. The aerodynamics solver supplies the drag properties that the performance analysis needs in order to run. In turn, the performance analysis supplies the Mach number that the aerodynamics discipline needs to compute the aircraft drag. Similar couplings are indicated between the other disciplines as well". [10]

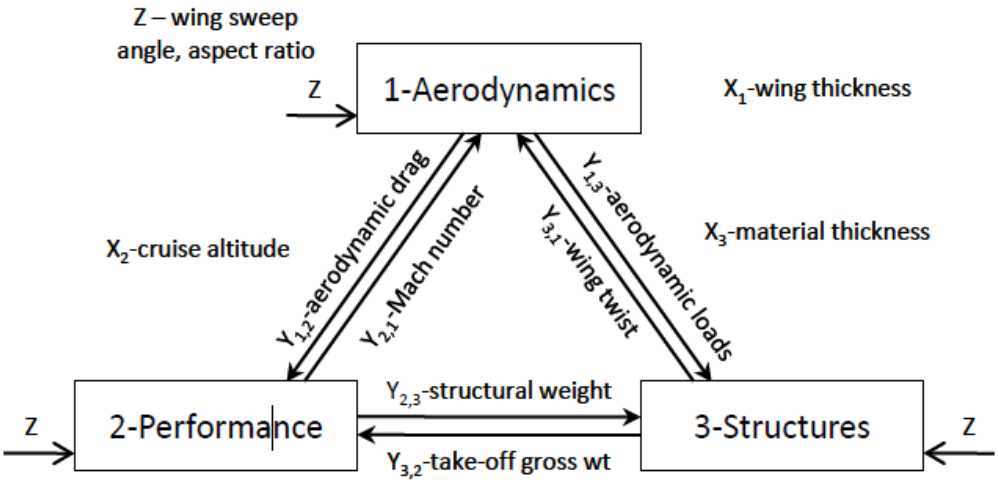

Figure 11: Coupled System Example

"The multidisciplinary nature of most design problems complicates model choice and implementation. Often several iterations are necessary between the disciplines in order to find the values of the objectives and constraints". [10]

Chapter three

Mathematical Model

Chapter three: Mathematical Model

3.1 The New Wing Combination Models:

3.1.1 Introduction

The models are equations that approximate and describe the response of the wing combination to the air loads. They are works together as **Frame** to define the wing combination. The wing combination divided into 6 stations: the first at the sliding part leading edge and the second after the sliding part trailing edge, the third at the rotor inlet while the fourth after its outlet, Stations 5 and 6 at the original wing leading and trailing edges respectively.

3.1.2 System of axes

The aircraft main axes are: X_{CG}, Y_{CG} and Z_{CG}. They pass through the aircraft center of gravity. Secondary axes had been used for simplicity of work such as: X, Y and $Z, X', Y'$and Z', $X'', Y''$and Z'' …etc. they are translated or rotated by angle from the main axes. Once the maneuver will be established from level flight, it will be achieved in short time and the fuel consumption will decrease as the aircraft deaccelerates and the fan build up to carry the aircraft; it is fair to take the aircraft mass to be constant during the maneuver besides, the only reason lead to the aircraft center of gravity shift is the extending of the sliding part which carry the fans mass which shift the CG forward into certain point, we took this point as a constant origin for the aircraft for simplicity where the axes X_{CG}, Y_{CG} and Z_{CG} located. Its location depends on the mass of the sliding part, the fans and their mass distribution. Thus, t had been estimated after the design of the sliding part and the modification of the fans and then the secondary axes were translated to that origin.

3.1.3 SU-35S wing aerodynamic model

Introduction

The wing aerodynamic model was needed to provide the values of:

- The wing total lift.
- The wing lift distribution.
- The wing total drag.
- The wing drag distribution.
- The wing aerodynamic moment produced by the total wing lift.

Since SU-35S is a fighter, it has a thin airfoil. The classical thin airfoil theory for a cambered airfoil had been used to model the wing for incompressible inviscid flow and then a correction for the compressibility effects, 3D-wing effects and the viscosity effects took place. To simulate the aerodynamic forces and moments distribution along the semi-span, the process had been repeated on finite number of sections (airfoils).

Generally, the classical thin airfoil theory is for inviscid incompressible irrational flow. But, below the stall angle of attack and at low airflow speeds over the airfoil, the actual experimental data for the lift and moment agrees very well with that values predicted by the inviscid classical thin airfoils theory, see table (5) which compares the experimental and theoretical data for NACA 23012 airfoil. In other word the classical thin airfoil theory cannot predict the flow separation. [27]

Since the small angle of attack are one of the maneuver constraint and the flow over the real wing below the 0.7 Mach, the using of the inviscid classical thin airfoils theory had been acceptable. [27]

Table 5: compares the experimental and theoretical data for NACA 23012 airfoil.

	Calculated by the classical thin airfoil theory	Experiment
$\alpha_{L=0}$	$-1.09°$	$-1.1°$
$C_l \; at \; = 4°$	0.559	0.55
$C_{m_{c/4}}$	-0.0127	-0.01

The flow over the wing is irrational because the wing receives axial flow from the rotor and because the angle of attack is small, the separation over the wing is inconsiderable. Thus, the thin airfoil theory and Prandtl-Glauert compressibility correction are available to use.

Model configuration

- **The axes**:

The axes used to model the wing are as follow: the wing has been modeled by three systems of axes, the first was used to estimate the lift at near root section (N_1) and it has the samples, $X, Y\ and\ Z$, while the other was used to simulate the lift distribution and it has the samples, $X', Y'\ and\ Z'$. The last one is used to estimate the chord distribution $X'', Y''\ and\ Z''$.

X: parallel to the axis X_{CG} with a shift distance of -2.28

Y: parallel to the axis Y_{CG} with a shift distance of …

Z: parallel to the axis Z_{CG} with a shift distance of …

Then, the local lift and drag effect at the near root and the tip section have been treated as a forces effects at points of the aerodynamic centers which have the Cartesian coordinates (x', y', z').

X': corresponding to the axes X_{CG}.

Y': parallel to the axis Y_{CG} with a shift distance of …

Z': parallel to the axis Z_{CG} with a shift distance of …

For the third system:

X'': rotated than the axis X_{CG} by 29 degrees with a shift distance of -2.28

Y'': rotated than the axis Y_{CG} by 29 degrees with a shift distance of …

Z'': parallel to the axis Z_{CG} with a shift distance of

- **Modeling process:**

The whole airfoil is approximated by the camber line and the effect of the airfoil shape on the flow is represented by a vortex sheet placed on the chord line in the plan (X-Z) and extended to a unit length along the Y-axis. See figure (12) below.

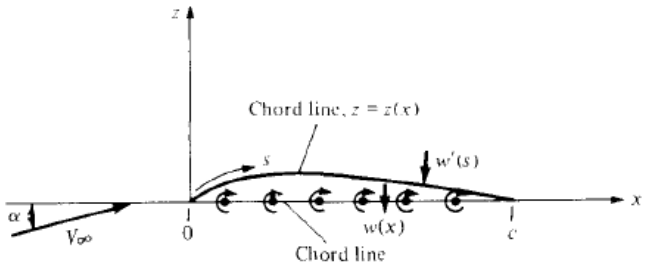

Figure 12: airfoil is approximated by the camber line.

This model is based on making the camber line a streamline in the flow. A vortex in the vortex line which extended span-wisely produce a velocity gradient and thus we can say it simulate the boundary layer and represent the viscosity effect.

A constraint on the using of the classical thin airfoil theory is that the angle of attack must be small (in radian) and this constraint considered in the optimization.

SU-35S has no aerodynamic twist. Thus the zero-lift angle of attack still constant. The zero-lift angle of attack has been estimated for near root section using the classical thin airfoil theory for cambered airfoils:

$$\alpha_{L=0} = -\frac{1}{\pi}\int_0^{\pi}\frac{dz}{dx}\,(cos\theta_0 - 1)\,d\theta_0 \;\ldots.\,(1)$$

To estimate $\frac{dz}{dx}$ for the thin airfoil smooth camber line at the near the root section, a second order equation is solved for its coefficients A, B and C to estimate z(x) at first:

$$Ax^2 + Bx + C = z(x) \;\ldots.\,(2)$$

Using the excel table (6) below:

Table 6: the near root section coordinates.

X	Z-upper surface	Z-lower surface	Camber line
0	0	0	0
0.002206	0.006618	-0.00551	0.000551
0.011029	0.014706	-0.01103	0.001838
0.036765	0.029412	-0.02206	0.003676
0.110294	0.047794	-0.03493	0.006434
0.147059	0.055147	-0.04044	0.007353
0.367647	0.088235	-0.05699	0.015625
0.551471	0.110294	-0.06985	0.020221
1.102941	0.147059	-0.09559	0.025735

1.470588	0.165441	-0.10846	0.028493
1.838235	0.176471	-0.11765	0.029412
2.205882	0.180147	-0.11765	0.03125
2.941176	0.165441	-0.11029	0.027574
3.67647	0.128676	-0.09191	0.018382
4.227941	0.084559	-0.05882	0.012868
4.595588	0.055147	-0.03676	0.009191
4.963235	0.025735	-0.01471	0.005515
5.279411	0	0	0

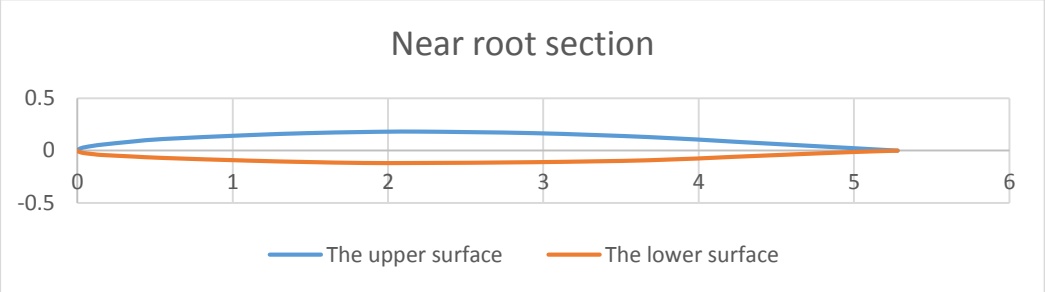

Figure 13:near root section.

Note: X- has been measured from the near root section leading edge in meters.

At $x = 0$: $z = 0$

$\Rightarrow C = 0$

At $x = 0.002206$: $z = 0.000551$

$\Rightarrow A(0.002206)^2 + B(0.002206) = 0.000551$ … (3)

At $x = 0.036765$: $z = 0.003676$

$\Rightarrow A(0.036765)^2 + B(0.036765) = 0.003676$ …. (4)

Solving equations (3) and (4) together:

$A = -2.591$
$B = 0.195$
$\Rightarrow Z(X) = -2.591\ X^2 + 0.195\ X$ …. (5)

Using this equation to calculate the Z coordinate of the camber line for the X values, the resulting camber line is corresponding to the real camber line except between [0:0.002206 m] and for accuracy purposes, the value of B has been adjusted to 0.250 through this sector. See figure (14) and (15).

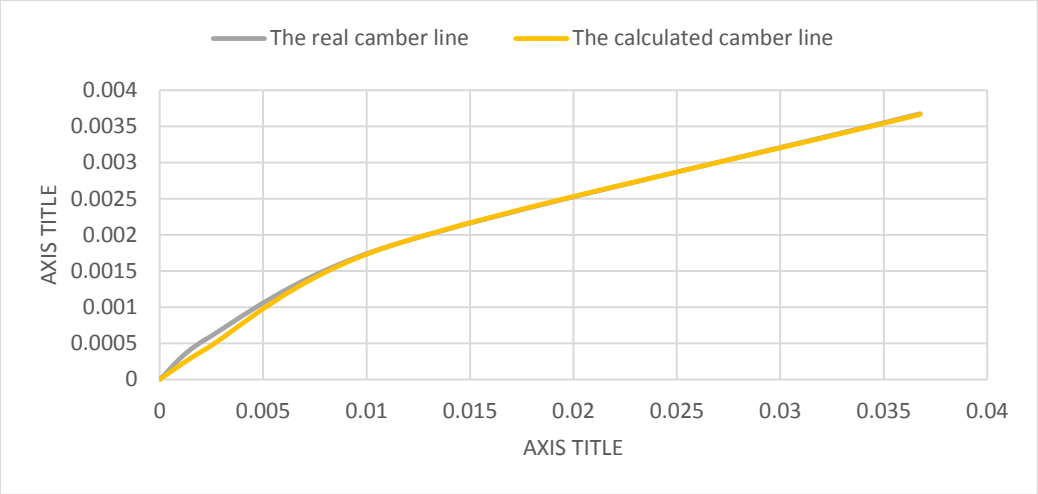

Figure 14: real and calculated camber lines.

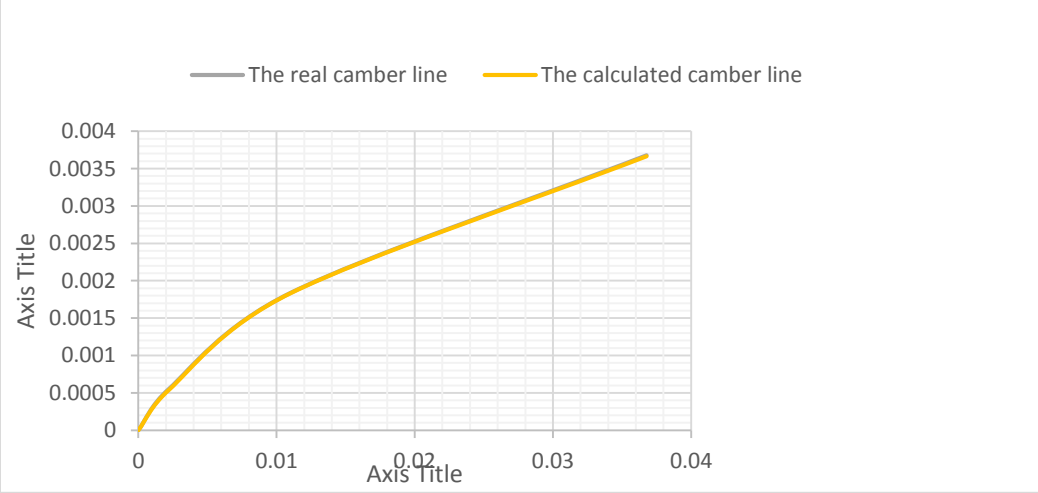

Figure 15: real and calculated camber lines.

Thus:

$$Z(X) = -2.591X^2 + \ 0.250X \Rightarrow \frac{dz}{dx} = -5.902\,x + 0.250, \quad for: 0 \le X \le 0.002206$$

$$Z(X) = -2.591\,X^2 + \ 0.195X \Rightarrow \frac{dz}{dx} = -5.902\,x + 0.195, \quad for: 0.002206 < X \le 0.036765$$

The procedure has been repeated along the chord line, and 6 equations had been estimated to describe the camber line:

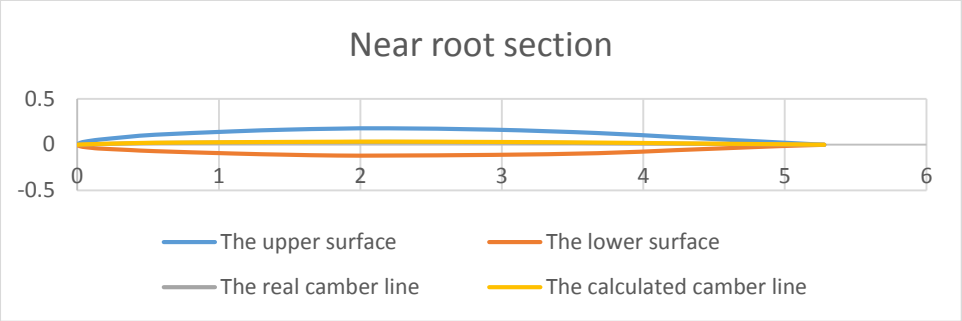

Figure 16: near root section camber line.

Table 7:

X limits	The equation	The derivation
$0 \leq X \leq 0.002206$	$-2.591X^2 + 0.250X$	$-5.902\,x + 0.250$
$0.002206 < X \leq 0.036765$	$-2.591\,X^2 + 0.195X$	$-5.902\,x + 0.195$
$0.036765 < X \leq 0.551471$	$-0.003X^2 + 0.036X + 0.003$	$-0.006x + 0.036$
$0.551471 < X \leq 2.205882$	$-0.003X^2 + 0.015X + 0.013$	$-0.006x + 0.015$
$2.205882 < X \leq 4.227941$	$-0.003X^2 + 0.011X + 0.022$	$-0.006x + 0.011$
$4.227941 < X \leq 5.279411$	$-0.007X^2 + 0.055X - 0.095$	$-0.014x + 0.055$

$\theta_0 = cos^{-1}\left(1 - 2\,\frac{x}{c}\right)$

At $x = 0\,m:\ \theta_0 = cos^{-1}\left(1 - 2\,\frac{0}{5.279411}\right) = 0\,rad.$

At $x = 0.002206\,m:\ \theta_0 = cos^{-1}\left(1 - 2\,\frac{0.002206}{5.279411}\right) = 0.041\,rad$

$\because x = \frac{C}{2}\,(1 - cos\theta_0) = \frac{5.279411}{2}\,(1 - cos\theta_0) = 2.639706\,(1 - cos\theta_0)$ … (6)

Substitute eq (6) in eq (5):

$\frac{dz}{dx}(\theta_0) = -5.902\,[2.639706\,(1 - cos\theta_0)\,] + 0.250 \qquad for:\ 0 < \theta_0 \leq 0.041\,rad.$

The procedure has been repeated for $0 < \theta_0 \leq \pi\,rad.$, see the table (4):

Table 8:

X limits	θ_0 limits	The derivation
$0 \le X \le 0.002206$	$0 < \theta_0 \le 0.041$	$-5.902\ [2.639706\ (1-\ cos\theta_0)\ ] + 0.250$
$0.002206 < X \le 0.036765$	$0.041 < \theta_0 \le 0.167$	$-5.902\ [2.639706\ (1-\ cos\theta_0)\ ] + 0.195$
$0.036765 < X \le 0.551471$	$0.167 < \theta_0 \le 0.658$	$-0.006[2.639706\ (1-\ cos\theta_0)\ ] + 0.036$
$0.551471 < X \le 2.205882$	$0.658 < \theta_0 \le 1.406$	$-0.006[2.639706\ (1-\ cos\theta_0)\ ] + 0.015$
$2.205882 < X \le 4.227941$	$1.406 < \theta_0 \le 2.216$	$-0.006[2.639706\ (1-\ cos\theta_0)\ ] + 0.011$
$4.227941 < X \le 5.279411$	$2.216 < \theta_0 \le 3.142$	$-0.014[2.639706\ (1-\ cos\theta_0)\ ] + 0.055$

$$\alpha_{L=0} = -\frac{1}{\pi}\left\{\begin{array}{l} \int_0^{0.041}[-5.902\ [2.639706\ (1-\ cos\theta_0)\ ] + 0.250]\ (cos\theta_0 - 1)\ d\theta_0 \\ + \int_{0.041}^{0.167}[-5.902\ [2.639706\ (1-\ cos\theta_0)\ ] + 0.195]\ (cos\theta_0 - 1)\ d\theta_0 \\ + \int_{0.167}^{0.658}[-0.006[2.639706\ (1-\ cos\theta_0)\ ] + 0.036]\ (cos\theta_0 - 1)\ d\theta_0 \\ + \int_{0.658}^{1.406}[-0.006[2.639706\ (1-\ cos\theta_0)\ ] + 0.015]\ (cos\theta_0 - 1)\ d\theta_0 \\ + \int_{1.406}^{2.216}[-0.006[2.639706\ (1-\ cos\theta_0)\ ] + 0.011]\ (cos\theta_0 - 1)\ d\theta_0 \\ + \int_{2.216}^{3.142}[-0.014[2.639706\ (1-\ cos\theta_0)\ ] + 0.055]\ (cos\theta_0 - 1)\ d\theta_0 \end{array}\right\}$$

$$= -\frac{1}{\pi}\ (0.000 + 0.000 - 0.003 + 0.010 + 0.007 + 0.024)$$

$$\alpha_{L=0} = -0.012\ \ rad. = \ -0.687\ degree$$

To consider the 3D wing effect in the local lift coefficient, replace α by the effective angle of attack:

Using Kuchemann formula for swept wings, the wing lift curve slope has been estimated:

$$a = \frac{a_o \cos \Lambda_{c/2}}{\sqrt{1+\left(\frac{a_o\ \cos \Lambda_{c/2}}{\pi e AR}\right)^2 + \left(\frac{a_o\ \cos \Lambda_{c/2}}{\pi e AR}\right)}} \quad \text{….. (7)}$$

$$= \frac{2\pi \cos(30.01)}{\sqrt{1+\left(\frac{2\pi \cos(30.01)}{\pi(0.742)(3.776)}\right)^2}+\left(\frac{2\pi \cos(30.01)}{\pi(0.742)(3.776)}\right)} = 3.02\ per\ rad.$$

Where:

The tapper ratio of SU-35S: $\lambda = \frac{C_t}{C_r}$ = 0.28, the induced drag factor $\delta = 0.016$, the span efficiency factor e_0:

$e_0 = \frac{1}{1+\delta} = 0.984$ …. (8)

Then, the Oswald efficiency factor which is for swept wings is given by the Hörner formula:

$e = e_o \cos \Lambda_{L.E.} = 0.984 \times \cos 49 = 0.646$ … (9)

Table 9:relation between angle of attack and lift coefficient.

α	cl	cd	cl/cd
-1	-0.086	0.020623	-4.17015
1	0.086	0.020623	4.170153
3	0.258	0.025605	10.07628
5	0.43	0.035569	12.08932
7	0.602	0.050514	11.91739
9	0.774	0.070442	10.98773
11	0.946	0.095352	9.921142
13	1.118	0.125244	8.926604
15	1.29	0.160117	8.056598

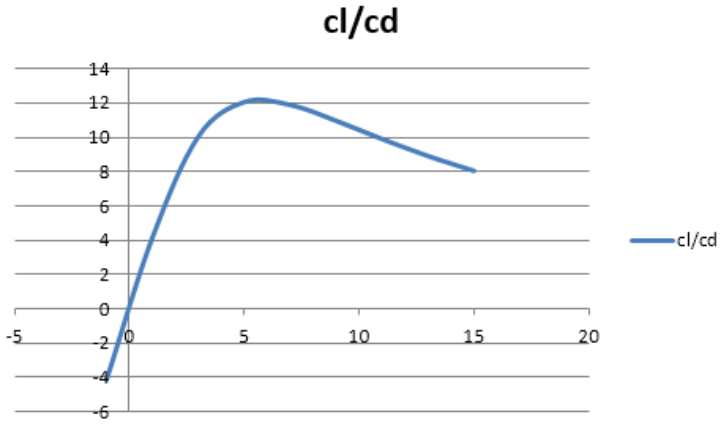

Figure 17: lift curve slop.

From table (9):

$$C_L = \frac{(0.946 - 0.774)}{(11 - 9)} = 0.086$$

The aerodynamic moment around the aerodynamic center: this moment is caused by the lift force. Once the lift force changes due to the wing tip vortex effect, this must be represented in the equation besides the compressibility effect. The location of the aerodynamic center for the wing section that the wing lift resultant effects has been estimated:

$$\bar{x}_{ac}(y) = -\frac{\frac{dC_{m,c/4}}{d\alpha}}{a_0} + \frac{1}{4} \quad \ldots\ldots (10)$$

Using the thin airfoils theory:

$$C_{m,c/4} = \frac{\pi}{4}(A_2 - A_1) \quad \ldots\ldots (11)$$

$$A_1 = \frac{2}{\pi}\int_0^{\pi} \frac{dz}{dx}\cos\theta_0 \, d\theta \quad \ldots. (12)$$

$$A_2 = \frac{2}{\pi}\int_0^{\pi} \frac{dz}{dx}\cos 2\theta_0 \, d\theta \quad \ldots\ldots (13)$$

"A_1 and A_2 depended only on the shape of the camber line and do not involve the angle of attack"." Thus, the quarter-chord point is the theoretical location of the aerodynamic center for a cambered airfoil".

$$\frac{dC_{m,c/4}}{d\alpha} = \frac{\pi}{4}\frac{d(A_2 - A_1)}{d\alpha} = 0 \quad \ldots\ldots (14)$$

$$\bar{x}_{ac}(y) = 0.25$$

To estimate the aerodynamic line sweep angle:

$$\Lambda_{ac} = 35\ degrees$$

The moment around the aerodynamic center:

$$C_{m,ac} = C_{m,c/4} = \frac{\pi}{4}(A_2 - A_1) = \text{constant}$$

$$A_2 = \frac{2}{\pi}(0.011 + 0.012 + 0.021 - 0.003 + 0.005 - 0.008) = 0.024$$

$$C_{m,ac} = \frac{\pi}{4}(0.024 - 0.035) = -0.009$$

Note:

$$cos2\theta_0 = \cos{\theta_0}^2 - 1$$

$$\bar{C} = \frac{2}{3} C_r \left[\frac{1+\lambda+\lambda^2}{1+\lambda}\right] \quad \ldots (15)$$

$= \frac{2}{3}\ (5.26)\left[\frac{1+(0.28)+(0.28)^2}{1+(0.28)}\right] = 3.72$

The drag produced by the wing,

$C_D = \ C_{D,0} + C_{D,i} + C_{D,w}$ … (16)

Since the maneuver such that the wing will receive a velocity below the critical Mach number; there is no wave drag over the wing:

$\therefore C_{D,w}$ = zero

$\therefore C_D = \ C_{D,0} + C_{D,i}$

$C_{D,i} = \ k_3 {C_L}^2$ … (17)

where: $k_3 = \frac{1}{\pi AR} = \ \frac{1}{\pi(\ 3.776)} = 0.0842$ …. (18)

$C_{D,i} = \ 0.0842\ {C_L}^2 = 0.0842\ (0.086)^2 = 0.0006$

$C_{D,0} = \ C_{D,e_0} + \ \Delta C_{D,0} = C_{D,e_0} + \ k_1 {C_L}^2$ …. (19)

$k_1 = \ \frac{1}{3}\ k_3 \ = \frac{0.0842}{3} = 0.028$ … (20)

Where $\Delta C_{D,0}$ is an increment in the zero lift drag due the separation happens by the increasing in the angle of attack to increase the lift coefficient.

$C_D = 0.02 + (0.028 + \ 0.0842){C_L}^2 = 0.02 + (0.112 * \ 0.086^2) = 0.021$

The total drag has been assumed to effect through the same point where the total lift effect, for simplicity of calculations. (the total lift effect at the point of the second moment of area point of the lift distribution shape along the semi-span, thus no need to estimate the drag distribution if the drag effect at the same point)

3.1.4 SU-35S stability model

It is important during maneuver to achieve a longitudinal stability to be sure the aircraft fly vertically not pitch. the main contributors are:

- The wing-body
- The horizontal tail
- The engines nacelles
- The fans
- The addition sliding part

Since SU-35S has a small wing-span-to-body-diameter ratio, the mutual interference between the wing and the fuselage is considerable. For such configuration we evaluate the wing-body together.

$C_{m_{\alpha,wb}} = \left(\bar{x}_{cg} - \bar{x}_{ac_{wb}}\right) C_{L_{\alpha,wb}}$ … (21)

To estimate the lift curve slope for the wing body combination:

$C_{L_{\alpha WB}} = \left[K_N + K_{W(B)} + K_{B(W)}\right] C_{L,\alpha e} \left(\frac{S_{exp}}{S}\right)$ …. (22)

$C_{L,\alpha e} = \frac{3.46}{\sqrt{M^2-1}}$ =1.72 …. (23)

S = 62 m^2

M= 2.25

$S_{exp} = 36.74\ m^2$

$K_N = \left(\frac{C_{L_{\alpha,N}}}{C_{L_{\alpha,e}}}\right) \left(\frac{S_{exp}}{S}\right)$ ….. (24)

$= \left(\frac{0.0973}{1.72}\right) \left(\frac{36.74}{62}\right) = 0.034$

For subsonic speeds:

$C_{L_{\alpha,N}} = \frac{2\,(k_2 - k_1)\, S_{B,max.}}{S}$ …. (25)

Using SU-35S data:

$S_{B,max.} = 3.6351\ m^2$ at station number 8.

$b_{f,max.} = 4.57\ m$

b = 15.3 m

$l_f = 21.9\ m$

Using figure (18) at fineness ratio: $\frac{l_f}{b_{f,max.}}$ = 4.79, the value of $k_2 - k_1 = 0.83$

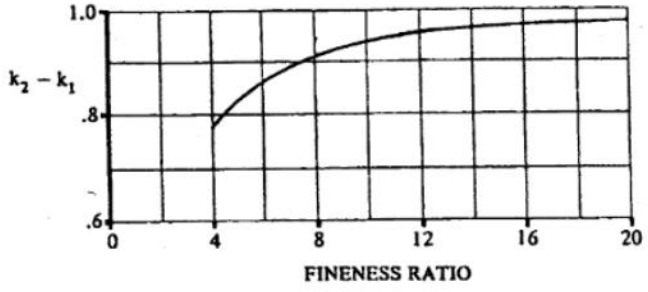

Figure 18: fuselage apparent mass coefficient.

$C_{L_{\alpha,N}} = \frac{2 \times 0.83 \times 3.6351}{62} = 0.0973$ per rad.

$\frac{b_{f,max.}}{b} = 0.3$

$K_{W(B)} = 0.1714 \left(\frac{b_{f,max.}}{b}\right)^2 + 0.8326 \left(\frac{b_{f,max.}}{b}\right) + 0.9974 = 1.26$ … (26)

$K_{B(w)} = 0.7810 \left(\frac{b_{f,max.}}{b}\right)^2 + 1.1976 \left(\frac{b_{f,max.}}{b}\right) + 0.0088 = 0.44$ …. (27)

$C_{L_{\alpha WB}} = [(0.034) + (1.26) + (0.44)](1.72)\left(\frac{36.74}{62}\right) = 1.77$

Now to estimate the value of $\bar{x}_{ac_{wb}}$:

$\left(\frac{x_{ac_{wb}}}{C_{re}}\right) = \frac{\left(\frac{x_{ac}}{C_{re}}\right)_N C_{L_{\alpha,N}} + \left(\frac{x_{ac}}{C_{re}}\right)_{W(B)} C_{L_{\alpha,W(B)}} + \left(\frac{x_{ac}}{C_{re}}\right)_{B(W)} C_{L_{\alpha,B(W)}}}{C_{L_{\alpha,WB}}}$ …. (28)

$C_{L_{\alpha,W(B)}} = C_{L_{\alpha,e}} K_{W(B)} \left(\frac{S_{exp}}{S}\right) = \frac{3.46}{\sqrt{1-M^2}} \times 1.26 \times \left(\frac{36.74}{62}\right) = \frac{2.58}{\sqrt{M^2-1}} = 1.28$ …. (29)

$C_{L_{\alpha,B(W)}} = C_{L_{\alpha,e}} K_{B(W)} \left(\frac{S_{exp}}{S}\right) = \frac{3.46}{\sqrt{1-M^2}} \times 0.44 \times \left(\frac{36.74}{62}\right) = \frac{0.90}{\sqrt{M^2-1}} = 0.45$ …… (30)

For subsonic speeds:

$\left(\frac{x_{ac}}{C_{re}}\right)_N = -\left(\frac{1}{C_{re}\, S_{B,max.}}\right) \int_0^{x_0} \frac{dS_b(x)}{dx} (l_N - x)\, dx$ … (31)

$C_{re} = 5.41\, m$

$l_N = 3.01\, m$

The nose sectional area is circular: $S_b(x) = \frac{\pi}{4} {D_N}^2$ where $D_N = f(x)$. Using the geometrical data of SU-35S:

Table 10:

X	D_N
0	0
1.2 m	0.90 m
3.01 m	1.38 m

It's clear that the, the diameter of the nose is change in a second order equation related to the change in x:

$Ax^2 + Bx + C = D_N(x)$ ….. (32)

At $x = 0 \Rightarrow C = D_N(0) = 0$

At $x = 1.2 \Rightarrow A(1.2)^2 + B(1.2) = 0.9$ ….. (33)

At $x = 3.01 \Rightarrow A(3.01)^2 + B(3.01) = 1.38$ …. (34)

Solving equation (33) and (34):

B = 0.943

A = - 0.161

$-0.161\,x^2 + 0.943\,x = D_N(x)$ … (35)

$S_b(x) = \frac{\pi}{4}\,{D_N}^2 = \frac{\pi}{4}\,[-0.161\,x^2 + 0.943\,x]^2 = \frac{\pi}{4}\,[(-0.161\,x^2)^2 - 2 \times 0.161\,x^2 \times 0.943\,x + (0.943\,x)^2] = \frac{\pi}{4}\,(0.026\,x^2 - 0.304\,x^3 + 0.889\,x^2)$ ….. (36)

$\frac{dS_b(x)}{dx} = \frac{\pi}{4}\,(0.026\,x^4 - 0.304\,x^3 + 0.889\,x^2) = \frac{\pi}{4}(0.104\,x^3 - 0.912\,x^2 + 1.778\,x)$

$\left(\frac{x_{ac}}{C_{re}}\right)_N = -\left(\frac{1}{5.41 \times 3.6351}\right) \int_0^{x_0} \left[\frac{\pi}{4}(0.104\,x^3 - 0.912\,x^2 + 1.778\,x)\right] (3.01 - x)\,dx =$

$-\left(\frac{\pi}{4 \times 5.41 \times 3.6351}\right) \left\{\int_0^{x_0}(0.313\,x^3 - 2.745\,x^2 + 5.352\,x)\,dx - \int_0^{x_0}(0.104\,x^4 - 0.912\,x^3 + 1.778\,x^2)\,dx\right\} = -0.040\,\left[\left(\frac{0.313\,x^4}{4} - \frac{2.745\,x^3}{3} + \frac{5.352\,x^2}{2}\right) - \left(\frac{0.104\,x^5}{5} - \frac{0.912\,x^4}{4} + \frac{1.778\,x^3}{3}\right)\right]$

$since\ \beta A_e\ for\ SU - 35S =$:

$\left(\frac{x_{ac}}{C_{re}}\right)_{B(W)} = \frac{1}{4} + \left(\frac{b - b_{f,max.}}{2C_{re}}\right) \chi \tan \Lambda_{c/4}$ …. (37)

$\tan \Lambda_{c/4} = 0.67$

The value of the parameter χ had been found from figure (19): $\chi = 0.266$

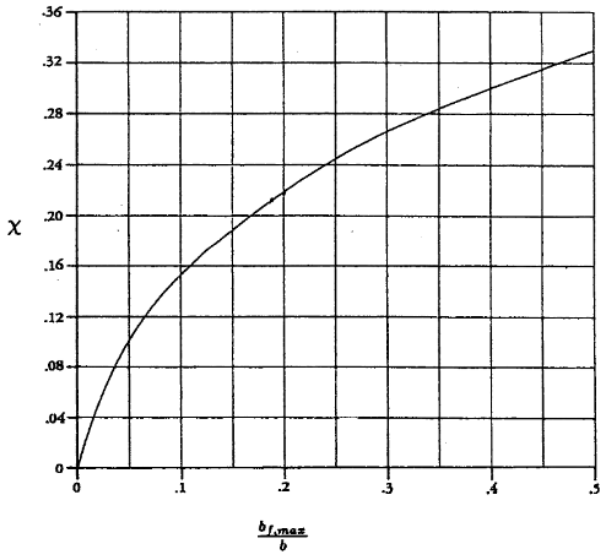

Figure 19: subsonic wing-lift carryover performance.

$$\left(\frac{x_{ac}}{C_{re}}\right)_{B(W)} = \frac{1}{4} + \left(\frac{15.3 - 4.57}{2 \times 5.41}\right) \times 0.266 \times 0.67 = 0.427$$

Since the effect of the body in the wing aerodynamic center is small and can be neglected:

$$\left(\frac{x_{ac}}{C_{re}}\right)_{W(B)} = \left(\frac{x_{ac}}{C_{re}}\right)_{W}$$

The tail is extremely impressed in the wing wake; thus the tail will receive high velocity as well as the wing even at the low aircraft speed. This makes the tail capable to trim the aircraft.

$$C_{m_{\alpha,t}} = -a_t \left(1 - \frac{d\epsilon}{d\alpha}\right) \eta_t V_t \quad \text{..... (38)}$$

The fuselage side flow (down wash) on the horizontal tail is small and can be neglected; because of the presence of the vertical tail as a wall prevent the fuselage side flow to reach the horizontal tail. In the other hand the wing is very close to the horizontal tail and affect it by considerable down wash.

Since as motioned before, the maneuver will be achieved in high subsonic speeds, we used the empirical formula for subsonic speeds to estimate:

$$\frac{d\epsilon}{d\alpha} = 4.44 \left[k_A k_\lambda k_H \left(\cos \Lambda_{1/4}\right)^{1/2}\right]^{1.19} \quad \text{.... (39)}$$

$$\cos \Lambda_{1/4} = 0.83$$

$$k_A = \frac{1}{AR} - \frac{1}{1 + AR^{1.7}} = \frac{1}{3.776} - \frac{1}{1 + 3.776^{1.7}} = 0.170 \quad \text{.... (40)}$$

$$k_\lambda = \frac{10 - 3\lambda}{7} = \frac{10 - (3 \times 0.28)}{7} = 1.309 \quad \text{..... (41)}$$

$$l_h = 4.81\ m$$

$$h_H = -0.6\ m$$

$$k_H = \frac{1 - \frac{h_H}{b}}{\sqrt[3]{\frac{2l_h}{b}}} = \frac{1 - \frac{-0.6}{15.3}}{\sqrt[3]{\frac{2 \times 4.81}{15.3}}} = \frac{1.039}{0.857} = 1.212 \quad \text{..... (42)}$$

$$\frac{d\epsilon}{d\alpha} = 4.44\left[0.170 \times 1.309 \times 1.212 \times (0.83)^{1/2}\right]^{1.19} = 0.836$$

As the vertical tail presence keep the fuselage cross flow away from the horizontal tail, the value of the tail lift curve slope is equal to the value of lift curve slope for isolated horizontal tail.

Since the maneuver had been achieved at subsonic speeds we used the Datcom below to estimate the dynamic pressure ratio:

$\eta_t = 1 - \frac{\Delta q}{q}$ ….. (43)

$l_{h1} = 2.467\ m$

$\bar{C} = 3.72\ m$

$\frac{\Delta q}{q} = \frac{2.42\sqrt{C_{D_{o,w}}}}{\frac{l_{h1}}{\bar{C}}+0.30} = \frac{2.42\sqrt{0.02+(0.028){C_L}^2}}{\frac{2.467}{3.72}+0.30} = 2.564\sqrt{0.02+(0.028){C_L}^2} = 0.36$ …. (44)

$\eta_t = 1 - 2.564\sqrt{0.02+(0.028)(0.086)^2} = 0.44$

$V_h = \frac{S_h\, l_h}{S\,\bar{C}} = \frac{(1.8)\,(2.467)}{(62)\,(3.72)} = 0.0193$

$AR = 3.92$

$e = \frac{1}{1+\delta} = \frac{1}{1+0.33}0.75$

$a_t = \frac{a_o \cos \Lambda_{c/2}}{\sqrt{1+\left(\frac{a_o\ \cos \Lambda_{c/2}}{\pi e AR}\right)^2}+\left(\frac{a_o\ \cos \Lambda_{c/2}}{\pi e AR}\right)}$ … (45)

$= \frac{2\pi \cos(32.38)}{\sqrt{1+\left(\frac{2\pi \cos(32.38)}{\pi(0.75)(3.92)}\right)^2}+\left(\frac{2\pi \cos(32.38)}{\pi(0.75)(3.92)}\right)} = 3.08\ per\ rad$

$C_{m_{\alpha,t}} = -a_t\left(1-\frac{d\epsilon}{d\alpha}\right)\eta_t V_t$ … (47)

$= -3.08(1-0.836)\left(1-2.564\sqrt{0.02+(0.028)(0.086)^2}\right)V_t$

$= -0.32(0.0193) = -0.0062$

The thrust produced by the two turbo-fan engine is relatively small during the maneuver to keep low forward speed; thus, it is acceptable to ignore the nacelles contribution.

The prop-fan effect in the longitudinal stability consist of:

- **Effect of thrust line vertical location related to the CG line**

  The prop-fan thrust effect through the thrust line in the direction of airflow. When a vertical distance separate between the thrust line and the CG line a pith down moment will produced around the aircraft CG. Once the distance between the CG line and the thrust line of the prop-fans is very small and the thrust produced by them approximately equal to zero.

  $M_{CG.propeller} = T_P . h_p$ …. (48)

  Divide equation (48) by qSC to estimate the moment coefficient around the CG:

$C_{m_{CG.RS}} = \frac{T_P}{q.s}\frac{h_p}{C}$ … (49)

$C_{m_{\alpha.RS}}$ = zero

The moment produced by the propeller forward thrust don't affected by the local flow angle of attack. This shows that, the effect of propeller thrust location relative to the location of the CG has neutral contribution in the aircraft stability.

- **Effect of the normal force**

The normal force is the vertical component of the thrust when the prop-fans experience a local freestream with angle of attack (α_p) and it produces pitch up moment around the CG for puller configuration (Destabilizing).

$M_{CG.RS} = N_P . l_p$ …. (50)

Divide equation No.3 by q.S.C to estimate the moment coefficient around the CG:

$C_{m_{CG.SR}} = \frac{N_P}{q.S}\frac{l_p}{C}$ … (51)

$C_{N_P} = \frac{N_P}{q.S_P}$ …. (52)

$C_{m_{CG.RS}} = \frac{C_{N_P} . q . S_P}{q . S}\frac{l_p}{C} = \frac{C_{N_P} . S_P}{S}\frac{l_p}{C}$ *****rvs CNP

$C_{m_{\alpha.RS}} = \frac{S_P}{S}\frac{l_p}{C}\frac{\partial C_{N_P}}{\partial \alpha_P}\frac{\partial \alpha_P}{\partial \alpha}$ … (53)

Once the prop-fans feed the wing with axial flow (no down or up wash) $\frac{\partial \alpha_P}{\partial \alpha} = 1$. Also, $\frac{S_P}{S} = 0.5\ or\ 1$ since the total upper surface of the wing is impressed in the prop-fans wake while the lower surface can be impressed in the prop-fans wake or not.

$C_{m_{\alpha.RS}} = \frac{S_P}{S}\frac{l_p}{C}\frac{\partial C_{N_P}}{\partial \alpha_P}\frac{\partial \alpha_P}{\partial \alpha}$

The normal force affected by the local flow angle of attack at small angle of attacks. So, it has a contribution in the aircraft $C_{m_{0,RS}}$ and in $\frac{\partial C_{m_{CG.RS}}}{\partial \alpha}$.

- **Effect of the slipstream (wake)**

The propeller slipstream passes over the wing and the horizontal tail. "the wing sections exposed to the propeller slipstream experience a high dynamic pressure and hence develop higher local lift and drag force". This increment in lift and drag is local (2-D lift and drag) and it make a distortion to the lift and thus drag

distribution over the wing leading to increase in the aerodynamic forces. This effect is small and can be neglected. But the tail is affected more than the wing because the propeller slipstream affects the tail efficiency (η) (the tail will experience much turbulent air flow if there a propeller than if there is no propeller and the tail angle of attack will increase) and also the downwash (ε), thus the horizontal tail lift to trim will be affected more.

Due to the increment in the wing lift by ΔL due to the prop-fans axial wake, additional moment around the aircraft center of gravity will be produced but the value of $C_{m_{\alpha,wb}}$ is the same as if there is no prop-fan axial wake.

The additional sliding part contribution effect in the other stability contributions through the shifting of the CG forward. And also by the increment in the lift ΔL. The sliding part-span-to-body-diameter ratio is small thus it had been treated individually.

$C_{m_{\alpha,sp}} = a_{sp}\left(\bar{x}_{cg} - \bar{x}_{ac_{sp}}\right)$ … (54)

Where: a_{sp} and $\bar{x}_{ac_{sp}}$ are design values.

3.1.5 SU-35S structural model

Introduction:

The structural model of SU-35S wing had been approximated using the idealization theory.

The objectives of the model:

This model aimed to achieve one objective: to be sure for the produced air loads, the wing bending stiffness and torsional stiffness are capable to be counteracted (resisted) these loads by considering the structural model in the optimization as constraints.

Assumptions:

1. The skin and the webs have been assumed to be fully effective in resisting the shear stresses.
2. The flanges and the stringers have been assumed to be fully effective in resisting the direct stresses.
3. Due to the lack of the data about the internal structure of the fighter SU-35S, the dimensions of the stringers and the three spars are approximated using a closer model of fighters. The stringers area chosen to be $900\ mm^2$ at the near root section

N_1 while the spars flanges are chosen to be $1200\ mm^2$ for the same section. The area decreases linearly even reach $600\ mm^2$ and $900\ mm^2$ at the tip for the stringers and the flanges respectively. Also, since it's so difficult to manufacture a variable thickness stringers or spars, the thickness of the them have been taken to be constant which means, the dimensions of the stringer or the spar are change along its length. The skin thickness has been chosen to be $0.8\ in$ and it's constant.

4. Since the dimensions of the wing internal structural element (such as a stringer section) are small, it's fair to take the moment of inertia for the section, $I_G = 0$.
5. Once the wing semi-span for SU-35S (as the most of the fighters) is relatively short, the wing flexibility is low (the wing is more rigid). Thus, the bending moment has been taken to vary linearly around the root.
6. No axial constraint effects (neglect the weapons, their fixations … etc.).

Air loads definitions:

The wing is a complex closed sections and it is affected by two main force and a moment. The forces as follow, the lift distribution resultant which effect at distance y_L in the Z-axis direction and the drag distribution resultant which effect parallel to the wing ribs (at the most of the wing) and normal to Spar No.2 which swept back by 29 degrees. Thus, it divided into two components: one parallel to the X-axis and the other parallel to the Y-axis. The moment is the aerodynamic moment produced by the transition of the lift resultant from the center of pressure of the airfoil section where the lift actually effects into the aerodynamic center of the same section. Both lift and drag forces incline by the angle of attack and the wing setting angle from the X-Y plane, thus both of them have contribution in the loads that affect the wing parallel to the X, Y and the Z axes.

Note, the wing total lift don't affect by the induced angle of attack.

- The load in the X direction ≡ $S_x = L\sin(\alpha + i_w) + D_x\cos(\alpha + i_w)$
- The load in the Y direction ≡ $S_y = D_y$
- The load in the Z direction ≡ $S_z = L\cos(\alpha + i_w) - D_x\sin(\alpha + i_w)$

Where:

$D_x = D\cos 29$

$D_y = D\sin 29$

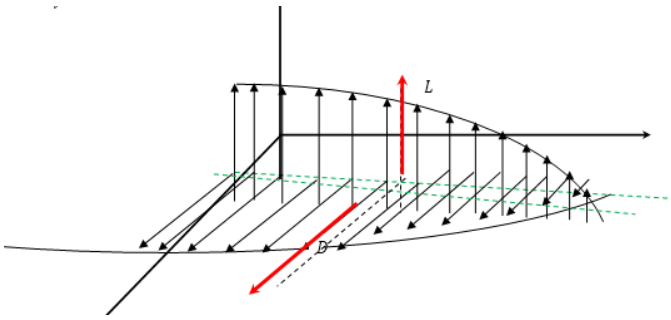

The force S_z bends the wing around the X-axis, produce a shear flow in the wing internal structure once it doesn't pass through the shear center of the wing sections (twisting) and it twists the wing about the Y-axis (that is because the wing is sweptback and thus the aerodynamic line where the lift distribution effects through sweptback also relative to the Y-axis, thus this force produce a moment in a plane parallel and pass through the sweptback aerodynamic line, this moment con be divided into two components: the first around the X-axis, bending while the other around the Y-axis, twisting) which produce additional shear flow in the wing structure. The force S_x and S_y exert an ignorable bending moment on the wing around the Z-axis and a considerable shear flow in the wing internal structure because they don't pass through the shear center of the wing sections (twisting).

The moment around the aerodynamic center has two components: the first twist the wing around the Y-axis producing a shear flow while the other bends the wing around the X-axis.

Shear centers estimation:

To estimate the shear center of each section: the shear center has coordinates $(\xi_s\ , \eta_s)$ the first in the $x$direction and the second in the z direction for a certain section at y. Case of zero twist and shear load effect through the shear center had been assumed. The moments around the leading edge of the section had been taken and equated with the internal moments due to the shear flow produced by this shear load.

Note: the shear centers have been estimated for sections all parallel to the X-axis.

To estimate ξ_s, unknown shear load $S_{\bar{z}}$ applied through the shear center.

The shear flow distribution due to any shear force S_z :

$$q_s = q_b + q_{s,o}$$

$$q_b = -\left(\frac{S_z\, I_{xz}}{I_{xx}\, I_{zz} - {I_{xz}}^2}\right) \left(\sum_{r=1}^{n} \beta_r\, x_r\right) - \left(\frac{S_z\, I_{zz}}{I_{xx}\, I_{zz} - {I_{xz}}^2}\right) \left(\sum_{r=1}^{n} \beta_r\, z_r\right)$$

The moment of inertia $I_{xx} = \sum \Delta I_{xx} = \sum_{r=1}^{N} \beta_r \, (\bar{z} - z\,)^2$

The moment of inertia $I_{zz} = \sum \Delta I_{zz} = \sum_{r=1}^{N} \beta_r \, (\bar{x} - x\,)^2$

The moment of inertia $I_{xz} = \sum \Delta I_{xz} = \sum_{r=1}^{N} \beta_r \, (\bar{x} - x\,)(\bar{z} - z\,)$

Where:

$\bar{z} = \frac{\Sigma(\beta.z)}{\Sigma\beta}$

$\bar{x} = \frac{\Sigma(\beta.x)}{\Sigma\beta}$

The shear flow in the five cuts $q_{S,O,R}$ is given by the rate of twist caused by these constant shear flow. Assume constant rate of twist:

$$\frac{d\theta}{dy} = \frac{1}{2A_R} \oint_R q \frac{ds}{t} = \frac{1}{2A_R} \oint_R \left(q_{S,O,R} + q_b\right) \frac{ds}{t}$$

$$\frac{d\theta}{dy} = \frac{1}{2A_1}\left[q_{S,O,1} \frac{ds_{I,IIc}}{t_{I,IIc}} + \left(q_{S,O,1} - q_{S,O,2}\right) \frac{ds_{I,II}}{t_{I,II}} + \oint_R q_b \frac{ds}{t}\right]$$

$$\frac{d\theta}{dy} = \frac{1}{2A_2}\left[-q_{S,O,1} \frac{ds_{I,II}}{t_{I,II}} + q_{S,O,2}\left(\frac{ds_{I,II}}{t_{I,II}} + \frac{ds_{I,III}}{t_{I,III}} + \frac{ds_{II,IV}}{t_{II,IV}} + \frac{ds_{III,IV}}{t_{III,IV}}\right) - q_{S,O,3} \frac{ds_{III,IV}}{t_{III,IV}} + \oint_R q_b \frac{ds}{t}\right]$$

$$\frac{d\theta}{dy} = \frac{1}{2A_3}\left[-q_{S,O,2} \frac{ds_{III,IV}}{t_{III,V}} + q_{S,O,3}\left(\frac{ds_{III,IV}}{t_{III,V}} + \frac{ds_{III,V}}{t_{III,V}} + \frac{ds_{IV,VI}}{t_{IV,VI}} + \frac{ds_{V,VI}}{t_{V,VI}}\right) - q_{S,O,4} \frac{ds_{V,VI}}{t_{V,VI}} + \oint_R q_b \frac{ds}{t}\right]$$

$$\frac{d\theta}{dy} = \frac{1}{2A_4}\left[\left(q_{S,O,4} - q_{S,O,3}\right) \frac{ds_{V,VI}}{t_{V,VI}} + q_{S,O,4} \frac{ds_{V,VI,c}}{t_{V,VI,c}} + \oint_R q_b \frac{ds}{t}\right]$$

The fifth equation which solved with the above five equations is the moment equation around the L.E:

$$S_z \xi = \sum_{R=1}^{4} M_{q,R} = \sum_{R=1}^{4} \oint_R q_b p ds + \sum_{R=1}^{4} 2A_R q_{S,O,R}$$

$\eta_s$has been estimated in a same manner but with applying unknown shear load S_x through the shear center. Then, the same procedure repeated.

The shear flow distribution due to the shear force S_x:

$$q_s = -\left(\frac{S_x I_{xx}}{I_{xx} I_{zz} - {I_{xz}}^2}\right) \left(\sum_{r=1}^{n} \beta_r \, x_r\right) - \left(\frac{-S_x I_{xz}}{I_{xx} I_{zz} - {I_{xz}}^2}\right) \left(\sum_{r=1}^{n} \beta_r \, z_r\right)$$

The moments taken around the leading edge of the section:

$$S_x \eta_s = \sum_{R=1}^{4} M_{q,R} = \sum_{R=1}^{4} \oint_R q_b p ds + \sum_{R=1}^{4} 2A_R q_{S,O,R}$$

Both S_z and S_x produce moment, the bending moment produced by S_x is around the Z-Axis and it usually neglected. SU-35S has high sweep thus, the force S_z produces

two moment components: the first is a bending moment and it is around the X-Axis call it M_x and the other around the Y-Axis call it M_y and it twist the wing down (torsion).

$M_y = S_z\, x_R$

$M_x = S_z\, y_R$

The moment around the aerodynamic center has two components: the first around the X-axis (bending moment) and the second around the Y-axis and it produces a torque. This torque generates a shear flow in the wing sections. This shear flow has a constant value for each cell of the section.

$M_y = M_{ac} \cos \Lambda_{ac} \; = M_{ac} \cos 35$

$M_x = M_{ac} \sin \Lambda_{ac} \; = M_{ac} \sin 35$

The structural analysis:

1. bending moment $\boldsymbol{M_x}$:

M_x is distributed along the semi-span between the wing root and the tip. The bending moment at any section is given by:

$M_x = S_z\,(y_R - y) + \; M_{ac} \sin 35$

$= \; [L \cos(\alpha + 1) - D \sin(\alpha + 1)\,](y_R - y) + \; M_{ac} \sin 35$

This bending moment generate direct stresses in the booms (stringers, the spar and ribs flanges). The direct stresses effects on the internal structural elements of the wing had been estimated for each element not for each section as follow:

❖ **direct stresses in booms**

The wing upper surface is tapered in two directions: $\alpha_u \neq 0 = 2$ and $\alpha_{L.E} \neq 0 = 42$ while the lower surface is tapered in one direction: $\alpha_l = 0$ and $\alpha_{T.E} \neq 0 = -14$. This tapering effects the stresses transmitting through the internal structural elements of the wing. The lower surface of the wing is not tapered in the y-direction. Thus, $\alpha_l = 0$ while $\alpha_u \neq 0$.

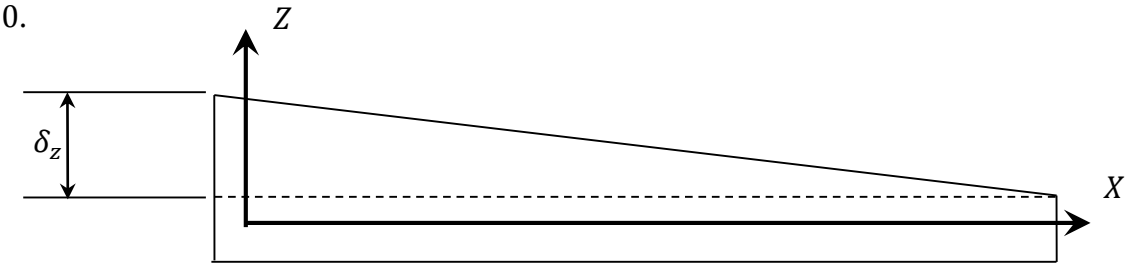

Each boom will experience an axial force p_r: for the upper surface booms of the wing this axial force p_{r_u}has three components: p_{r_x} , p_{r_y} , and p_{r_z}. p_{r_y} cause the direct stress σ normal to the boom area while p_{r_z} and p_{r_x}cause a shear stresses tangentially to the boom area. For the lower surface booms, the axial force p_{r_l} has two components: p_{r_x} , p_{r_y}. p_{r_y} cause the direct stress σ normal to the boom while p_{r_x} cause a shear stress in the boom area.

The direct stress at a section locates at distance y and has a moment of inertia I_{xx} due to the bending moment value at the section:

$\sigma_{y_r} = \frac{M_x(y)}{I_{xx}} z_r$

The max σ_{y_n} along the boom length must be less than the yield stress of the boom material to prevent permanent deformation of the booms. Thus,

$\sigma_{y_n} < \sigma_{yield}$

❖ **Shear stress in walls and webs**

The shear loads S_z and S_x produce shear flow in the walls and the webs besides p_{r_z} and p_{r_x} at the booms:

$S_{x,w}$ _ the shear flow resultant of the skin.

$S_{z,w}$ _ the shear flow resultant of the web.

$S_x = S_{x,w} + \sum_{r=1}^{n} p_{x,r}$

$p_{r_x} = \sigma_{y_{\beta,r}} \beta, r \frac{\delta_{xr}}{\delta_y}$

$S_z = S_{z,w} + \sum_{r=1}^{n} p_{z,r}$

$p_{r_z} = \sigma_{y_{\beta,r}} \beta, r \frac{\delta_{zr}}{\delta_y}$

$\frac{\delta_{xr}}{\delta_y} = \frac{\delta_{zr}}{\delta_y} = \begin{cases} \tan 2 & for\ the\ upper\ surface\ booms \\ 0 & for\ the\ lower\ surface\ booms \end{cases}$

The shear flow distribution in the panels due to S_x :

$q_b = -\left(\frac{S_{x,w} I_{xx} - S_{z,w} I_{xz}}{I_{xx} I_{zz} - {I_{xz}}^2}\right) \left(\int_0^s t_D \ x \ ds + \sum_{r=1}^{n} \beta_r \ x_r\right) -$

$\left(\frac{S_{z,w} I_{zz} - S_{x,w} I_{xz}}{I_{xx} I_{zz} - {I_{xz}}^2}\right) \left(\int_0^s t_D \ z \ ds + \sum_{r=1}^{n} \beta_r \ z_r\right)$

Using assumption number:

$\int_0^s t_D \; x \, ds = \int_0^s t_D \; z \, ds = 0$

$q_b = -\left(\frac{S_{x,w} I_{xx} - S_{z,w} I_{xz}}{I_{xx} I_{zz} - I_{xz}^{\;2}}\right) \left(\sum_{r=1}^{n} \beta_r \, x_r\right) - \left(\frac{S_{z,w} I_{zz} - S_{x,w} I_{xz}}{I_{xx} I_{zz} - I_{xz}^{\;2}}\right) \left(\sum_{r=1}^{n} \beta_r \, z_r\right)$

Because the booms have a variable cross-section are along their length additional shear value is added to the shear flow. This value is given as the change in the load p_{z_r} between two section separated by 35 even 70 cm. here, 50cm has been taken

$\Delta p = \frac{(p_{z_r})_y - (p_{z_r})_{y-0.5}}{y-(y-0.5)} = \frac{1}{2}\left[\left(p_{z_r}\right)_y - \left(p_{z_r}\right)_{y-0.5}\right]$

To predict the value of $q_{S,OR}$: the external moments due to the shear loads must be totally resisted by the internal moments produced by the internal shear flow. the moment is taken around point c due to the shear loads:

$S_{x,w}\eta - S_{z,w}\xi = \sum_{R=1}^{4} \oint_R \; q_b \, p_0 \, ds \; + \sum_{R=1}^{4} 2 \, A_R \, q_{s,o,R} \; - \sum_{r=1}^{n} p_{z_r} \xi_r + \sum_{r=1}^{n} p_{x_r} \eta_r$

2. The torsion

T(y)=$S_z \, (x_R - x) \; + \; M_{ac} \cos 35 = [L \cos(\alpha + 1) - D \sin(\alpha + 1)](x_R - x) +$

$M_{ac} \cos 35$

$T(y) = \sum_{R=1}^{4} 2 A_R q_R \; = 2A_1 q_1 + 2A_2 q_2 + 2A_3 q_3 + 2A_4 q_4$

Assuming a constant rate of twist:

$\frac{d\theta}{dy} = \frac{1}{2A_R} \oint_R \; q \; \frac{ds}{t}$

R = 1,2, …4 since SU-35S has three main spars.

Applying this equation for four sections:

$\frac{d\theta}{dy} = \frac{1}{2A_1}\left[q_1 \frac{ds_{I,IIc}}{t_{I,IIc}} + (q_1 - q_2)\frac{ds_{I,II}}{t_{I,II}}\right]$

$\frac{d\theta}{dy} = \frac{1}{2A_2}\left[-q_1 \frac{ds_{I,II}}{t_{I,II}} + q_2\left(\frac{ds_{I,II}}{t_{I,II}} + \frac{ds_{I,III}}{t_{I,III}} + \frac{ds_{II,IV}}{t_{II,IV}} + \frac{ds_{III,IV}}{t_{III,IV}}\right) - q_3 \frac{ds_{III,IV}}{t_{III,IV}}\right]$

$\frac{d\theta}{dy} = \frac{1}{2A_3}\left[-q_2 \frac{ds_{III,IV}}{t_{III,V}} + q_3\left(\frac{ds_{III,IV}}{t_{III,V}} + \frac{ds_{III,V}}{t_{III,V}} + \frac{ds_{IV,VI}}{t_{IV,VI}} + \frac{ds_{V,VI}}{t_{V,VI}}\right) - q_4 \frac{ds_{V,VI}}{t_{V,VI}}\right]$

$\frac{d\theta}{dy} = \frac{1}{2A_4}\left[(q_4 - q_3)\frac{ds_{V,VI}}{t_{V,VI}} + q_4 \frac{ds_{V,VI,c}}{t_{V,VI,c}}\right]$

By solving the five equations, the additional shear stress value can be obtained.

The shear stress effect the internal component must be below the yield shear stress of the components material.

$\tau = \frac{q}{t}$

3.2 The sliding parts conceptual design:

3.2.1 Design requirements:

1. The (sliding part + fans) weight must as possible moves the CG within the CG limits to be sure the stabilizer already found can cancel the new destabilizing effect.
2. Cl_{max} wing combination $\geq Cl_{max}$ wing.
3. a combination $\geq$ a wing, to get high lift coefficient as possible at low AOA.
4. T max comb = T max wing, to prevent any extra compressibility effect due to the shape.
5. Suitable volume to be retracted inside the wing structure and suitable also for fan size.
6. Keep the highest part of the fan flow over the wing upper surface and serve some of it into the lower surface in the cause of bad flow plan.
7. The sliding part L.E should have the same shape as the wing L.E, to reduce any extra drag due to the change in leading edge shape.

The sliding part should be suitable volume to be retracted inside the wing structure of SU-35 and suitable also for fan size. So it maximum thickness should be less than 0.28m at root, and less than 0.11m at the root.

The sliding part should cover all the area at the L.E from root to tip (5.25m).

The sliding part chord should store in the space between the L. E and the first spar. its length at the root should be less than 1.5m, and at tip should be less than 0.6m. so as to be retracted in the wing structure without cutting the first spar.

The sliding parts shape should have the same airfoil shape of SU-35 wing (NASA23012) to prevent any increase in drag due to the shape change.

Table 11: sliding parts design parameters.

Sliding part root chord	1.5 m
Sliding part tip chord	0.55 m
Max thickness of S.P at root	0.28 m
Max thickness of S.P at tip	0.11 m
S.P thickness/chord ratio	0.18
S.P sweep angle	49degree

3.3 The Fan conceptual design:

3.3.1 Fan design requirements:

- D < 0.28 root
- D < 0.11 tip
- Solid fan blade
- Fan volume should be suitable for the storages in sliding part.

Fan diameter: The fan diameter should be less than 0.28m at root, and less than 0.11m at root. In each wing there should be at least 7 fans in order to allow the flow to pass through all the area in the upper surface.

Blade airfoil: The blades airfoil selected from NASA supersonic through flow fan hub airfoil. (increases the velocity about 0.4 Mach)

Number of Blades (B):

There are many parameters must be taken in consideration at the number of blade selection, like diameter of the propeller. Since the rpm and angular velocity are not large and the fans diameters are small. And because the most efficient propellers are two bladed. We assumed that the number of blades are two blades.

Table 12: fan design parameters.

No of fans in each wing	7
D1	0.25 m
D2	0.22 m
D3	0.2 m
D4	0.17 m
D5	0.14 m
D6	0.11 m
D7	0.09 m
Number of blades	2
Rotational speed	17 189 rpm
Angular velocity	1800 rad/sec

$$n = 17\ 189\ rpm$$

$$\omega = \frac{2\pi n}{60} = \frac{2 \times \pi \times 17189}{60} = 1800\ rad/sec$$

To prevent stall propeller tip Mach number must be less than 1

$$\frac{V_{tip}}{a} > 1$$

$$V_{tip} \leq a$$

$$a = V_{tip} = \sqrt{\gamma RT} = \sqrt{1.4} \times 287 \times 288 = 340.174\ \ m/sec$$

$V_{tip} = \omega R$ =1800×(0.25/2)= 225 m/sec

$$M = \frac{V_{tip}}{a} = \frac{225}{340} = 0.66$$

3.3.2 The doors:

To prevent any increase in drag in the upper surface, the doors should be kept in the leading edge lower surface, it should open out ward of the wing structure leaving enough space for the sliding part to come out from the storage in the wing structure. then it closed while sliding part will be still hinged in horizontal position.

3.3.3 The sliding mechanisms:

The leading edge bottom door will open and the sliding part will extend out of the wing structure, until it reaches the specified position then it fixed at horizontal position, then the fans which stored in the sliding part will move backward into the original wing leading edge until it reaches the specified positon and it rotate accelerating the flow in the wing upper surface.

3.4 Drawing of the incorporation:

drawing of the sliding parts and fan and incorporation of additional parts in to su-35 CAD model.

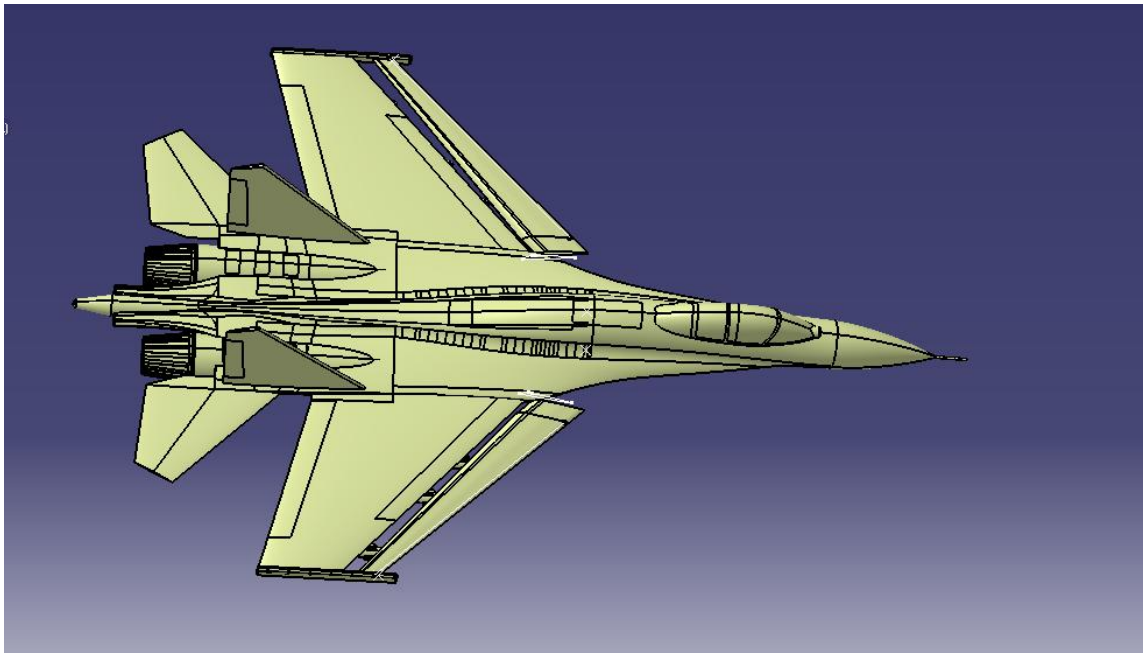

Figure 20:sukhoi-35 wing combination model.

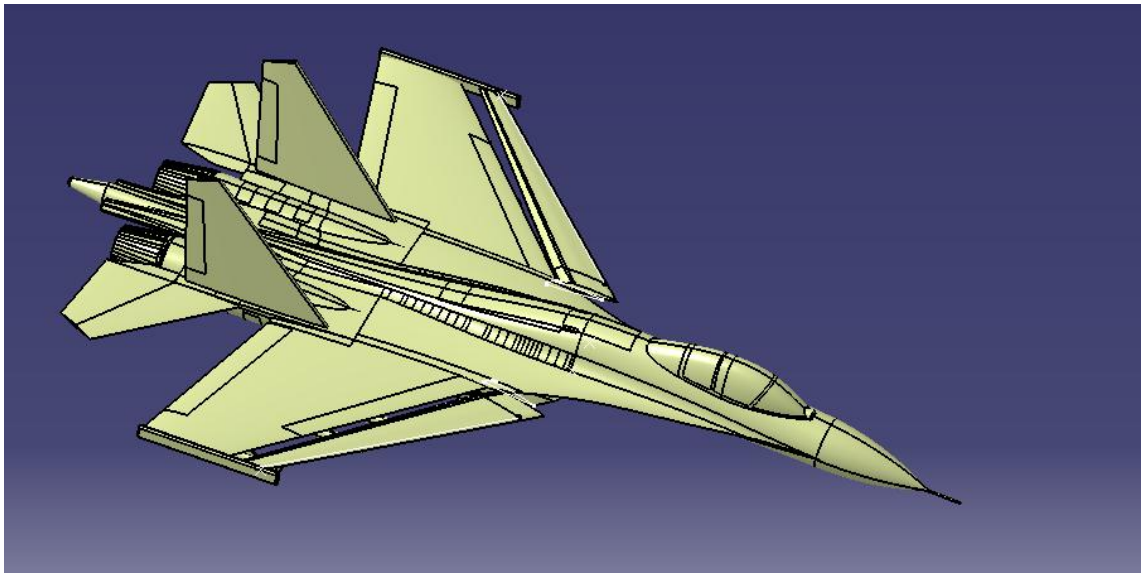

Figure 21:sukhoi-35 wing combination model.

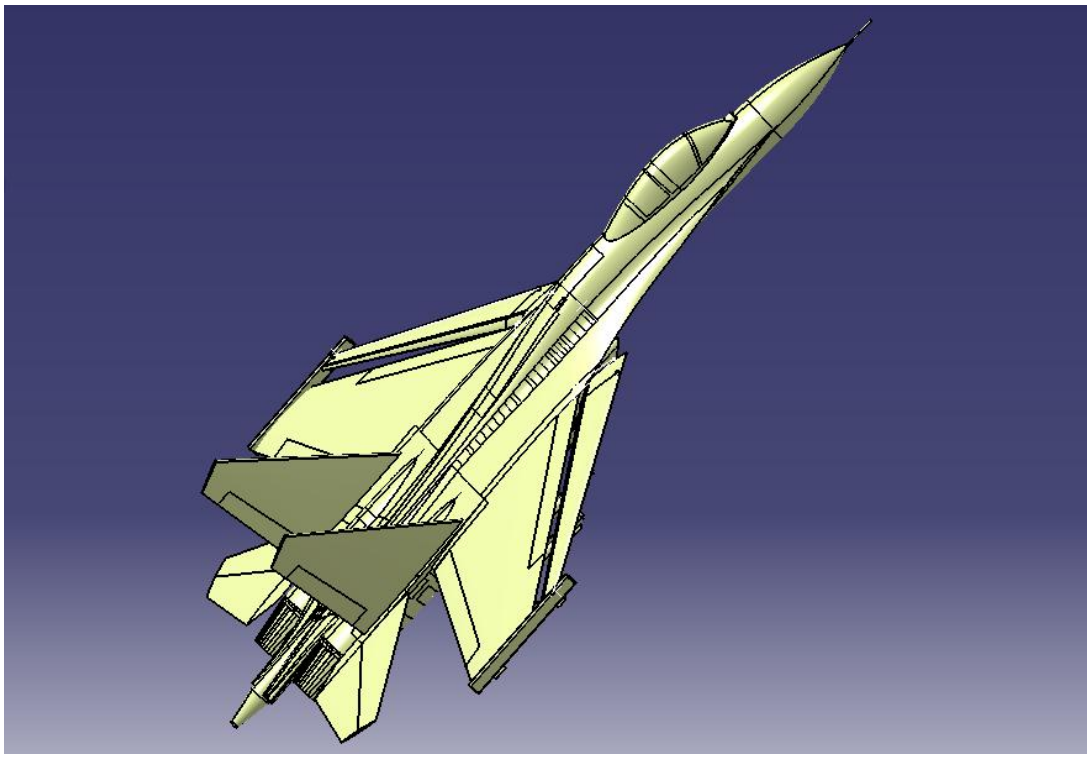

Figure 22:sukhoi-35 wing combination model.

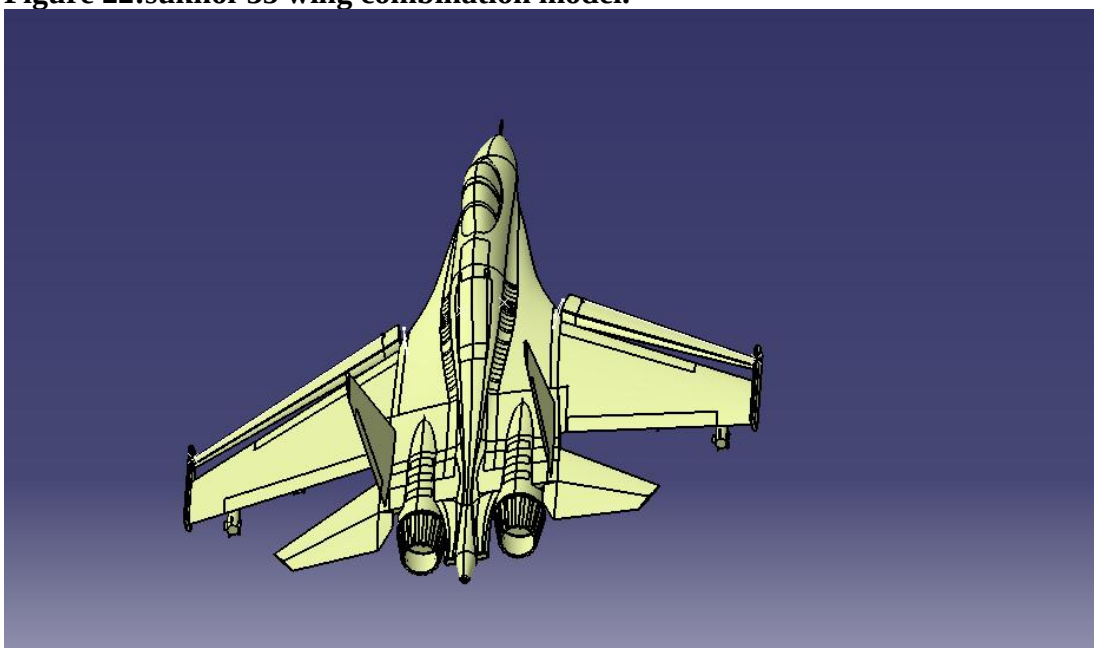

Figure 23: sukhoi-35 wing combination model.

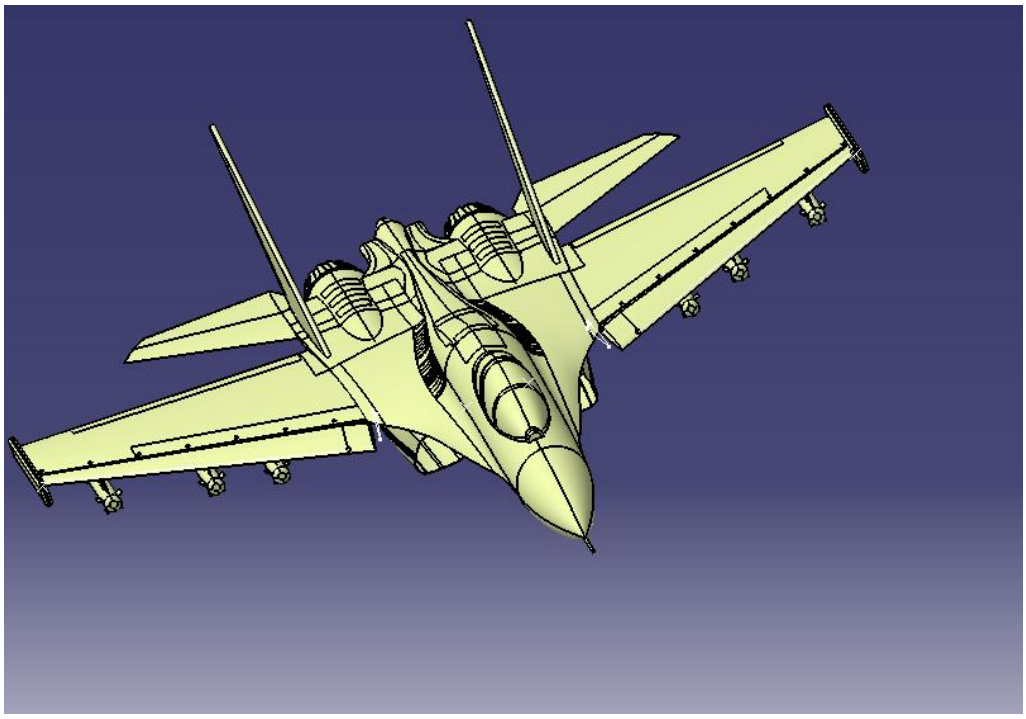

Figure 24:sukhoi-35 wing combination model.

Chapter four

Results and Discussion

Chapter four: Results and Discussion

4.1 Analytical results:

Sukhoi-35 mathematical models had been estimated analytically, starting with aerodynamic model using thin airfoil theory and aerodynamics, structural model using idealization and a simple stability model to check longitudinal stability. And the results shown in table (13).

Table 13: analytical results.

$\boldsymbol{\alpha_{L=0}}$	-0.012 rad, -0.648 degree
a	3.02 per rad
Λ	0.28
e_0	0.984
e	0.646
$\bar{x}_{ac}(y)$	0.25
$C_{m,ac}$	-0.09
C_L	0.086
k_3	0.0842
k_1	0.028
$C_{D,i}$	0.0006
C_D	0.021
$C_{L_{\alpha,N}}$	0.0973 per rad
$\bar{C}$	3.72
$\frac{d \in}{d\alpha}$	0.836
a_t	3.08 per rad
k_A	0.170
k_λ	1.309
k_H	1.212

$K_{W(B)}$	1.26
$K_{B(w)}$	0.44
$C_{L,\alpha e}$	1.72 per rad
K_N	0.034
$C_{L_{\alpha WB}}$	1.77
$C_{L_{\alpha,W(B)}}$	1.28
$C_{L_{\alpha,B(W)}}$	0.45
$\left(\frac{x_{ac}}{C_{re}}\right)_{B(W)}$	0.427
η_t	0.44
V_h	0.0193
$C_{m_{\alpha,t}}$	- 0.0062

4.2 CFD results:

Computational analysis had been done at these flight conditions:

- At cruise altitude (11000 m), temperature (216.65 k).
- At cruise velocity 2.25 Mach (663.68 m/s).
- At zero angle of attack (α= 0).
- Fan increases the velocity to 2.75 Mach (811.17 m/s).

4.2.1 Wing without fan:

cl= 0.017326534

cd= 0.001489378

cm at 0.25 = -0.020168859

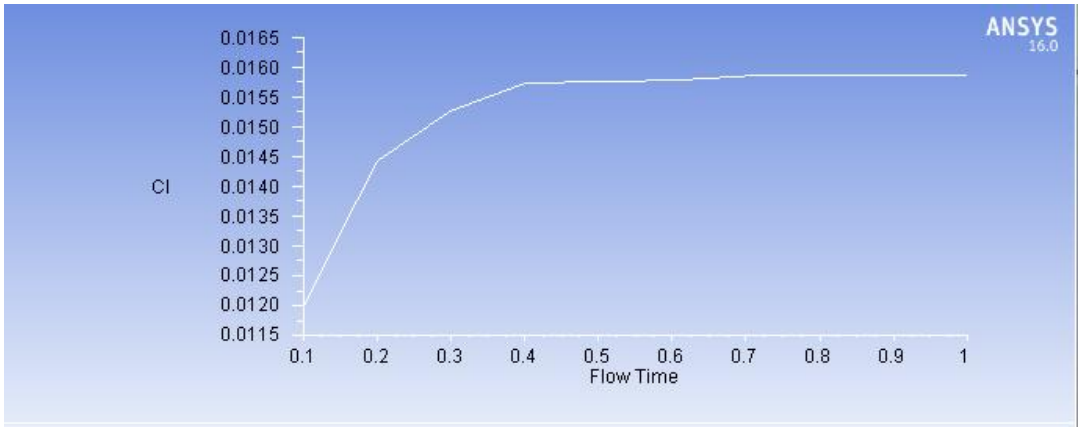

Figure 25: the change in lift coefficient with flow time.

The figure (25) represent the change in lift coefficient with the flow time for the original wing without fan, the lift coefficient increases as the flow time increase.

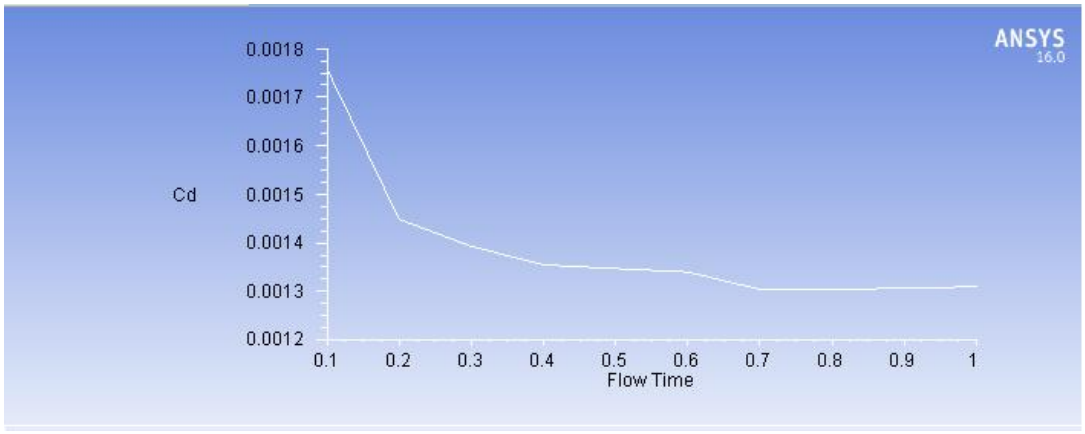

Figure 26: the change in drag coefficient with flow time.

The figure (26) represent the change in drag coefficient with the flow time for the original wing without fan, the drag coefficient decrease as the flow time increase.

4.2.2 Wing with fan:

cl = 0.026279672

cd= 0.0022173863

cm at 0.25 = -0.030597058

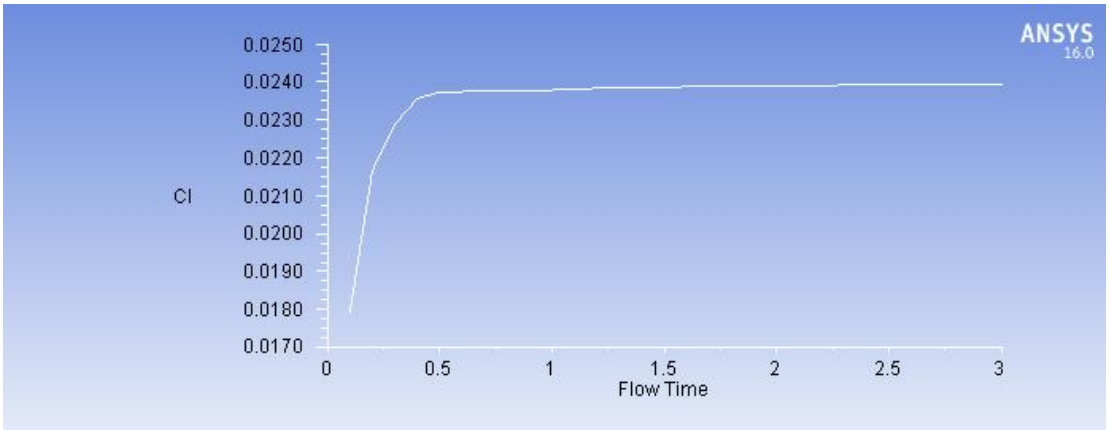

Figure 27:the change in lift coefficient with flow time.

The figure (27) represent the change in lift coefficient with the flow time for the new wing with fans, the lift coefficient increases as the flow time increase.

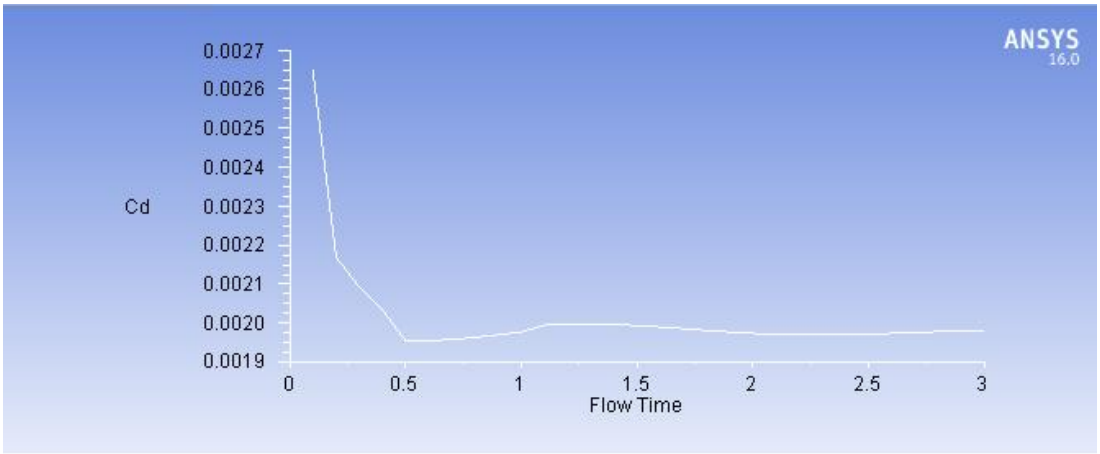

Figure 28: the change in drag coefficient with flow time.

The figure (28) represent the change in drag coefficient with the flow time for the new wing with fans, the drag coefficient decreases as the flow time increase.

From CFD results we noticed that the lift coefficient will increase when using fans (0.0148- 0.022). And the drag coefficient will increase slightly (0.0017- 0.0026).and the aerodynamic moment around quarter chord point increases when using fan (-0.02 to -0.03).

Chapter five

Conclusion, Recommendation and Future Work

Chapter five: Conclusion, Recommendation and Future Work

5.1 Conclusion:

In order to allow for sukoi-35 to perform this maneuver new parts had been designed that its function is to increase the wing lift and allow sukhoi-35 to perform the vertical flight maneuver.

The sukhoi-35 models had been estimated (aerodynamic, stability and structural model). Then the sliding parts had been conceptually designed by defining its airfoil shape and dimensions, and then the fan dimensions had been determined, then both of the sliding parts and fans had been drawn in CATIAv5 and had been incorporated into the sukhoi-35 CAD model. Then a computational aerodynamic analysis had been done around the wing section before and after using fans using CFD (fluent) and then the results had been discussed.

5.2 Recommendation:

We recommend to redo the computational analysis around the whole aircraft at different altitudes, design the fan (detail design) and design the internal structure for both wing and sliding parts.

5.3 Future work:

Future studies of this project should include the computational aerodynamic analysis for the whole aircraft, the detail design of the sliding parts and fans, reinforcing the week parts in the wing structure and simulation of the maneuver.

Appendixes A: Sukhoi-35 specification

Wing root chord	5.26 m
Wing tip chord	2.06 m
Length	21.9 m (72.9 ft)
Wingspan:	15.3 m (50.2 ft
Thickness/chord ratio	0.056
Wing loading	408 kg/m² (500.8 kg/m² with full internal fuel) (84.9 lb/ft² 50% fuel)
Height	5.90 m (19.4 ft)
Wing area	62.0 m² (667 ft²)
Dry thrust	8,800 kgf (86.3 kN, 19,400 lbf) each
Thrust with afterburner	14,500 kgf (142 kN, 31,900 lbf) each
Fuel capacity	11,500 kg (25,400 lb) internally
Service ceiling	18,000 m (59,100 ft)
Rate of climb	280 m/s (55,000 ft/min)
Thrust/weight	1.13 at 50% fuel (0.92 with full internal fuel)
Maximum *g*-load	+9 *g*
Maximum speed at altitude	Mach 2.25 (2,390 km/h, 1,490 mph)
Maximum speed at sea level	Mach 1.15 (1,400 km/h, 870 mph)
Leading edge sweep	49 degree

Appendixes B: NASA23012 coordinates

X	y
1.00003	0.00126
0.9973	0.0017
0.98914	0.00302
0.97563	0.00518
0.95693	0.00812
0.93324	0.01176
0.90482	0.01602
0.87197	0.02079
0.83506	0.02597
0.79449	0.03145
0.7507	0.03712
0.70417	0.04285
0.65541	0.04854
0.60496	0.05405
0.55335	0.05924
0.50117	0.06397
0.44897	0.06811
0.39733	0.0715
0.34681	0.07402
0.29796	0.07554
0.25131	0.07597
0.20738	0.07524
0.16604	0.0732
0.12732	0.06915
0.0923	0.06265
0.06203	0.05382
0.0373	0.04324
0.01865	0.03176
0.00628	0.0203
0.00015	0.00956
0	0
0.00533	-0.00792
0.01557	-0.01401
0.03029	-0.0187
0.04915	-0.02248
0.07195	-0.02586

0.09868	-0.02922
0.12954	-0.03282
0.16483	-0.0366
0.20483	-0.04016
0.24869	-0.04283
0.29531	-0.04446
0.34418	-0.0451
0.39476	-0.04482
0.4465	-0.04371
0.49883	-0.04188
0.55117	-0.03945
0.60296	-0.03655
0.6536	-0.03327
0.70257	-0.02975
0.7493	-0.02607
0.7933	-0.02235
0.83407	-0.01866
0.87118	-0.01512
0.9042	-0.0118
0.93279	-0.0088
0.95661	-0.00621
0.97543	-0.0041
0.98901	-0.00254
0.99722	-0.00158
0.99997	-0.00126
1	0

References

1. Anderson, J.D., aircraft performance and design 1999.
2. http://en.m.wikipedia.org/wiki/Harriier_Jump_Jet
3. http://en.m.wikipedia.org/wiki/Ducted_Fan
4. ntrs.nasa.gov, analysis of Mach 0.8 Turboprop slipstream wing
5. http://militaryrussia.ru/blog/topic-533.html
6. William J. Fredericks, CONCEPTUAL DESIGN OF A VERTICAL TAKEOFF AND LANDING UNMANNED AERIAL VEHICLE WITH 24-HR ENDURANCE, NASA Langley Research Center, Hampton, VA 23681
7. James F. Schmidt, D. Moore, Jerry R. Wood, Ronald J. Steinke, supersonic through-flow fan design, Lewis Research center, Cleveland Ohio, ntrs.nasa.gov, report.
8. Su-35 multifunctional super-maneuverable fighter www.SUKHOI.org.
9. Kopp, D.C., Sukhoi KnAAPO Su-35BM / Su-35-1 / Su-35s Flanker August, 2009.
10. MULTIDISCIPLINARY AIRCRAFT CONCEPTUAL DESIGN OPTIMIZATION CONSIDERING FIDELITY UNCERTAINTIES
11. https://en.wikipedia.org/wiki/Multidisciplinary_design_optimization
12. http://www.neos-guide.org/optimization-tree
13. https://en.wikipedia.org/wiki/Surrogate_model
14. http://www.neos-guide.org/content/optimization-introduction
15. Daniel_P._Raymer_Enhancing_Aircraft_Conceptual_Design_Using_Multidisciplinary_Optimization.
16. Advanced_Aircraft_Design__Conceptual_Design,_Technology_and_Optimization_of_Subsonic_Civil_Airplanes-Wiley_(2013)
17. https://en.wikipedia.org/wiki/Tiltrotor
18. https://en.wikipedia.org/wiki/Powered_lift#Fan-in-wing
19. https://en.wikipedia.org/wiki/Coand%C4%83_effect
20. https://en.wikipedia.org/wiki/Blown_flap
21. https://en.wikipedia.org/wiki/Circulation_control_wing
22. https://en.wikipedia.org/wiki/Leading-edge_extension
23. https://en.wikipedia.org/wiki/Focke-Achgelis_Fa_269

24. https://en.wikipedia.org/wiki/Slipstream

25. MORPHING WING DESIGN FOR UAVs:A PROPOSED CONCEPT , MABY BOADO AMADOR VAINATEY KULKARNI

26. https://en.wikipedia.org/wiki/Thrust_vectoring

27. Anderson,FUNDAMENTALS_OF_AERODYNAMIC

28. Aircraft_structures_for_engineering_students